CZECH TECHNICAL
UNIVERSITY
IN PRAGUE

FACULTY
OF MECHANICAL
ENGINEERING

# MASTER'S
# THESIS

2020

ADAM
KRUPICA

CZECH TECHNICAL
UNIVERSITY
IN PRAGUE

FACULTY
OF MECHANICAL
ENGINEERING
DEPARTMENT OF PROCESS
ENGINEERING

# MIXING IN SPHERICAL REACTORS AND TANKS

## MASTER'S THESIS

**Written by: Bc. Adam Krupica**
**Assigned by: Prof. Ing. Tomáš JIROUT, Ph.D.**

**2020**

# ZADÁNÍ DIPLOMOVÉ PRÁCE

## I. OSOBNÍ A STUDIJNÍ ÚDAJE

Příjmení: **Krupica** Jméno: **Adam** Osobní číslo: **475069**

Fakulta/ústav: **Fakulta strojní**

Zadávající katedra/ústav: **Ústav procesní a zpracovatelské techniky**

Studijní program: **Energetika a procesní inženýrství**

Specializace: **Procesní inženýrství**

## II. ÚDAJE K DIPLOMOVÉ PRÁCI

Název diplomové práce:

**Míchání v kulových reaktorech a zásobnících**

Název diplomové práce anglicky:

**Mixing in spherical reactors and tanks**

Pokyny pro vypracování:

• Zpracujte literární rešerši zaměřenou na proces míchání v nestandardních geometriích reaktorů a zásobníků a zaměřte se zejména na míchání v nádobách kulového tvaru.
• Na základě modelových experimentů stanovte základní charakteristiky míchání v kulových reaktorech a zásobnících. Zaměřte se zejména na proces homogenizace a suspendace v míchané vsádce.
• Výslekdy vyhodnoťte ve formě vhodných procesních charakteristik.
• Porovnejte účinnost míchání v kulových reaktorech a zásobnících s různou konfigurací procesu. Posuďte, zda a s jakou přesností je možné využít znalosti o procesu míchání v nejčastěji užívané konfiguraci s válcovou nádobou na inženýrský návrh míchání v zařízeních s nádobou kulového tvaru.

Seznam doporučené literatury:

Dle pokynů vedoucího práce.

Jméno a pracoviště vedoucí(ho) diplomové práce:

**prof. Ing. Tomáš Jirout, Ph.D. ústav procesní a zpracovatelské techniky FS**

Jméno a pracoviště druhé(ho) vedoucí(ho) nebo konzultanta(ky) diplomové práce:

Datum zadání diplomové práce: **20.04.2022** Termín odevzdání diplomové práce: **05.08.2022**

Platnost zadání diplomové práce: **18.09.2022**

| prof. Ing. Tomáš Jirout, Ph.D.<br>podpis vedoucí(ho) práce | prof. Ing. Tomáš Jirout, Ph.D.<br>podpis vedoucí(ho) ústavu/katedry | doc. Ing. Miroslav Španiel, CSc.<br>podpis děkana(ky) |
|---|---|---|

## III. PŘEVZETÍ ZADÁNÍ

Diplomant bere na vědomí, že je povinen vypracovat diplomovou práci samostatně, bez cizí pomoci, s výjimkou poskytnutých konzultací. Seznam použité literatury, jiných pramenů a jmen konzultantů je třeba uvést v diplomové práci.

. Datum převzetí zadání

Podpis studenta

# STATEMENT OF ORIGINALITY

I hereby declare that the present master's thesis was composed by myself and that the work contained herein is my own. All the assistance received in preparing this thesis and all the sources have been acknowledged.

Prague ……. ……

Bc. Adam Krupica

# Acknowledgement

I would like to thank my supervisor Prof. Ing. Tomáš Jirout, Ph.D. for all the time spent evaluating and discussing the contents of this thesis and for all the advice he has provided me with. I would also like to thank my family for enabling me to focus on my studies and for the overwhelming amount of support which they have provided me with over the years.

# Annotation sheet

**Name of the author:** Adam Krupica

**Title Czech:** Míchání v kulových reaktorech a zásobnících

**Title English:** Mixing in spherical reactors and tanks

**Scope of work:** number of pages: 71

number of figures: 26

number of tables: 6

number of appendices: 0

**Academic year:** 2021/2022

**Language:** English

**Department:** Department of Process Engineering

**Specialization:** Process Engineering

**Supervisor:** Prof. Ing. Tomáš JIROUT, Ph.D.

**Reviewer:**

**Tutor:** -

**Annotation - Czech:** Tato práce obsahuje energetické zhodnocení tří různých procesů míchání v kulových nádobách. Mezi vybrané metody patří míchání pomocí míchadel, proudu kapaliny a pomocí plynu. Dále byla vyhodnocena schopnost míchadel zajistit vznos částic.

**Annotation - English:** In this thesis, the energy assessment of 3 different mixing methods in spherical vessel was conducted. The chosen methods were agitator mixing, fluid mixing and pneumatic mixing. Additionally, the ability of the agitators to suspend particles was also tested.

**Keywords:** Mixing, Spherical vessel, Agitator mixing, Jet mixing, Sparger mixing, homogenisation

**Utilization:** The thesis can be utilized as groundwork for further research in this topic and for basic design of mixing device suitable for spherical vessels.

# Contents

# Abbreviations

| | | | | | |
|---|---|---|---|---|---|
| Abrv. | - | Abbreviation | MRT | - | Mean residence time |
| eq. | - | Equation | N-S | - | Navier – Stokes |
| g. | - | Gauge pressure | RPM | - | Rotations per minute |

# Agitators' nomenclature

| | | |
|---|---|---|
| A310 | - | Ligtnin® A310 agitator |
| FB3 | - | Pitched 3-blade impeller, with diagonally folded blades |
| FB6 | - | Pitched 6-blade impeller, with diagonally folded blades |
| PB6 | - | Pitched 6-blade impeller, blade angle: 45° |
| RT6 | - | Rushton turbine, 6 blades |
| VJ3 | - | Visco Jet® agitator |

# Characteristic numbers

| | | | | | |
|---|---|---|---|---|---|
| Da | - | Damköhler number | $Re_p$ | - | Pipe Reynolds number |
| Po | - | Power number | $Re_v$ | - | Vessel Reynolds number |
| Re | - | Agitator Reynolds number | | | |

# Physical quantities

| | | |
|---|---|---|
| A | Regression parameter | |
| B | Regression parameter | |
| $c_A$ | Molar concentration | (mol/m$^3$) |
| $c_A^0$ | Molar concentration at the beginning of the process | (mol/m$^3$) |
| $c_A^f$ | Molar concentration at the end of the process | (mol/m$^3$) |
| $c_V$ | Volume concentration of particles | (% vol.) |
| $c_p$ | Specific heat capacity | (J/Kg.K) |
| c* | Dimensionless molar concentration | (-) |
| d | Diameter of the impeller | (mm) |
| $d_p$ | Inner diameter of the pipe | (mm) |
| $d_s$ | Diameter of the sparger | (mm) |
| D | Diameter of the vessel | (mm) |
| $D_B$ | Diameter of the base of the sphere | (mm) |
| $D_t$ | Diameter of the top opening of the sphere | (mm) |

| | | |
|---|---|---|
| $e_k$ | Specific kinetic energy | (J/Kg) |
| $e_z$ | Specific energy loss | (J/Kg) |
| $\vec{f}$ | Body acceleration | ($m/s^2$) |
| $\vec{F}$ | Force vector | (N) |
| $h_p$ | Height of the particle cloud | (mm) |
| H | Fluid height | (mm) |
| $H_2$ | Agitator height above the bottom | (mm) |
| $H_S$ | Height of the sphere | (mm) |
| $H_{2s}$ | Sparger height above the bottom | (mm) |
| $\overrightarrow{J_A}$ | Molar flux | ($mol/s.m^2$) |
| $k_M$ | Torque value constant | (N.m/V) |
| $k_r$ | Reaction velocity constant | (L/mol.s) |
| L | Length of the uninterrupted jet stream | (m) |
| $\vec{n}$ | Vector of the surface direction | (-) |
| n | Rotation speed | (1/min) |
| $n_s$ | Just-suspended rotation speed | (1/min) |
| p | Pressure | (Pa) |
| $p_t^*$ | Dimensionless pressure in the developed turbulent region | (-) |
| $p_c^*$ | Dimensionless pressure in the creeping flow region | (-) |
| P | Power consumption | (W) |
| $\vec{q}$ | Heat flux | ($W/m^2$) |
| $\dot{Q}$ | Internal heat generation | ($W/m^3$) |
| $R_A$ | Production rate | ($mol/s.m^3$) |
| $S_B$ | Blade surface | ($m^2$) |
| $S_j$ | Cross section of the jet | ($m^2$) |
| S* | Dimensionless blade surface | (-) |
| t | Time | (s) |
| $t_h$ | Homogenisation time | (s) |
| $t_b$ | Blending time | (s) |
| t* | Agitator dimensionless time | (-) |
| $t_p^*$ | Pipe dimensionless time | (-) |
| $t_v^*$ | Vessel dimensionless time | (-) |
| T | Temperature | (K) |

| | | |
|---|---|---|
| $\vec{u}$ | Velocity vector | (m/s) |
| $\vec{u}^*$ | Dimensionless velocity vector | (-) |
| $\vec{u}_V^*$ | Vessel dimensionless velocity vector | (-) |
| $\bar{u}$ | Mean nozzle velocity | (m/s) |
| $\bar{v}$ | Mean jet velocity at the cross section | (m/s) |
| $\dot{V}$ | Volumetric flow | ($m^3/s$) |
| $\vec{x}$ | Coordinates | (m) |
| $\vec{x}^*$ | Dimensionless coordinates | (-) |
| $\vec{\vec{\delta}}$ | Unit tensor | (-) |
| $\vec{\vec{\Delta}}$ | Rate of strain tensor | (1/s) |
| $\varepsilon$ | Power density | ($W/m^3$) |
| $\mu$ | Dynamic viscosity of the liquid | (Pa.s) |
| $\rho$ | Density of the fluid | ($kg/m^3$) |
| $\vec{\vec{\sigma}}$ | Stress tensor | (Pa) |
| $\vec{\vec{\tau}}$ | Shear stress tensor | (Pa) |

# Introduction

Mixing is a procedure often used in the process industry, as it can shorten the necessary retention time of the fluid, hence lowering the required volume of a vessel or enabling intensification of a process.

Another desired outcome of mixing is the prospect of homogeneity of a batch, a crucial property that is often supposed when dealing with complex problems such as reactor heating or chemical reactions, as it elevates the necessity of fully describing the distribution of state functions. Other applications such as particle suspension, blending of fluids, creation of emulsions, also require mixing because the desired outcome is a fluid with uniform properties suitable for subsequent processing.

The main methods of mixing are the utilization of a mechanical agitator or a jet of fluid. A pneumatic system may also be used. These processes are highly dependent on the positioning, type of mixer and the geometry of the vessel but are usually well described for the most common type, the cylindrical vessel.

This thesis aims to apply the experimental methods found in the literature to evaluate the performance of various mixing methods on a spherical vessel, since there is a small amount of information available for this geometry.

Spherical vessels are used mainly as storage tanks for liquids, such as water or liquified gases. They are used because of their improved aesthetics and good resistance to the elements. Their additional advantage is the ability to withstand higher internal pressure than a cylindrical vessel with an equivalent diameter [1]. Another field of use is as anaerobic digesters [2]. In both cases, mixing is required to ensure the homogeneity of the product or to facilitate the supply of nutrients to the microbes.

The thesis is focused on the homogenisation process. To assess the performance of different methods of mixing, the required homogenisation energy will be used. The suspension of particles is also explored as it is often used in its industrial applications. Finally, an assessment will be made, whether the characteristic numbers of agitators gained on cylindrical vessels can be used on spherical vessels.

# 1 Theory of mixing

In the following chapters, the theoretical foundation for the evaluation of the experiments carried out in this thesis will be established. First, fundamental equations governing the process are introduced to show the constraints to which the evaluation of the methods must adhere to. Then the general theory for different methods of mixing is introduced.

## 1.1 Fundamental Equations

Mixing is a complex, three-dimensional, nonstationary problem of a multiphase fluid or an unhomogenized mixture which can be described through partial differential equations. These equations describe the conservation of mass, momentum, and energy. Supposing that the fluid is incompressible, the system can be described using six differential equations (1)-(4). Such a system is hard to solve as many of the variables depend on one another. More importantly, the equations themselves are usually very nonlinear.

$$(\vec{u} \cdot \nabla)\rho = 0 \tag{1}$$

$$\rho\left(\frac{\partial \vec{u}}{\partial t} + (\vec{u} \cdot \nabla)\vec{u}\right) = -\nabla p + \Delta \cdot \vec{\tilde{\tau}} + \rho\vec{f} \tag{2}$$

$$\left(\frac{\partial c_A}{\partial t} + (\vec{u} \cdot \nabla)c_A\right) = -\nabla \cdot \overrightarrow{J_A} + R_A \tag{3}$$

$$\rho c_p\left(\frac{\partial T}{\partial t} + (\vec{u} \cdot \nabla)T\right) = -\nabla \cdot \vec{q} + \vec{\tilde{\tau}} : \vec{\overrightarrow{\Delta}} + \dot{Q} \tag{4}$$

However, depending on the type of fluid and the method of mixing, the equations can be simplified, enabling an easier assessment of the problem. The method often used for the assessment is the dimensionless analysis. The possible simplifications are presented in the subsequent paragraphs.

The first assumption is that the temperature is constant throughout the whole volume and for the duration of the experiment. Consequently, the energy balance equation (4) can be disregarded. Hence, material properties, such as viscosity and diffusion coefficients, may also be considered constant.

To simplify the momentum equation (2) two modifications were applied. First, the effect of external forces was ignored. Second, the Newtonian behaviour of the fluid defined by the constitutive equation (5) was assumed, so a Navier-Stokes equation (6) without the term of the external forces was created.

$$\vec{\tau} = 2\mu\vec{\Delta} \tag{5}$$

$$\rho\left(\frac{D\vec{u}}{Dt}\right) = -\nabla p + \mu\nabla^2\vec{u} \tag{6}$$

Lastly, the material transport equation (3) can also be simplified. According to the Handbook of Industrial Mixing [3], in a stirred vessel, the main means of transportation is convection, enhanced by turbulence. Molecular diffusion is also present, but it is dominant on the microscale, as it is more effective at distances shorter than the size of the smallest vortices. On the contrary, at the macro scale, the diffusion term can be disregarded. If a chemical reaction is present, its term is much more problematic as it depends on the nature of the reaction. The Damköhler number (eq. (7)) can be used to assess whether the reaction time is insignificant compared to the mixing time [4]. Supposing that the value of Da is greater than 100, the reaction can be described as very fast, and hence the blending time is predominantly influenced by the speed of convection, allowing the omission of the reaction term. Combining both simplifications, the final simplified form of the transport equation (8) is presented.

$$Da = k_r c_A t_h \tag{7}$$

$$\left(\frac{\partial c_A}{\partial t} + (\vec{u}\cdot\nabla)c_A\right) = 0 \tag{8}$$

Although meticulous in nature, it is important to understand the limits imposed by the simplifications, since the experiments presented in the latter part of this thesis must adhere to these limitations. For example, if the reaction used in chapter 2.1 was significantly slower, we would not be able to disregard the effect of the reaction on the transport equation and, consequently, we would not be able to use the simplified equation (8). An example of a process, where the reaction kinetics dominate over the homogenisation time, would be fermentation, where low intensity, intermittent mixing can produce better results than continuous mixing [5], as the process is more governed by its biological nature than by the homogeneity of the batch.

## 1.2 Methods of mixing

As was discussed in the introduction, several different methods can be used to mix a liquid. In the thesis, three different methods are explored, namely, mixing using an agitator, a jet of liquid, or a sparger. The methods are compared using their energy requirement to achieve homogeneity. The energy is obtained as the product of the homogenisation time and the required power input. The best method will be chosen on the basis of this assessment.

As one of the uses found in the literature is the suspension of bacteria in anaerobic digesters, the ability to suspend particles will also be explored. For this purpose, only agitators were used, as no other method was capable to suspend the chosen particles. However, this is mainly due to the setup of the experiment, in reality, jets are more than capable to suspend particles as was proved by Kale and Patwardhan in [6].

### 1.2.1 Mixing in different vessel geometries

Three different vessel types are commonly used in the process industry. Starting with the most common one, the cylindrical vessel. Its dominance is caused by partially offering the benefits of the other two geometries. Due to its rotational symmetry, it is capable to withstand higher pressures, compared to rectangular vessels, while preserving part of its compact nature. As was mentioned in the Introduction, there is an abundance of data in the literature on cylindrical vessels and their various configurations. An example of the amount of data available is the often cited Handbook of industrial mixing [3] and the accompanying Advances in Industrial Mixing [7]. In general, large reviews on recent advances in the field of mixing are published for this geometry, such as the review published by Böhm et al. [8] on the topic of multiphase stirred reactors or the review by You et al. [9] on the Multiple-impeller stirred vessels.

Rectangular vessels are typically used as storage silos for granular or powdery substances as they can be efficiently packed but have problems to resist pressure [10]. The other typical use of this geometry is with concrete ponds often found in waste water treatment plants [11], or in aquaculture [12]. In these applications, particle suspension or mass transfer is often necessary. Due to the fragile nature of the living organism, jet or sparger systems are often used. Hence, the effects of sparger systems were described by Machina and Bewtra [13] and by Akhtar et al. [14]. Regarding agitation, it was shown that the corners of the vessel have the effect of baffles [3]. Additionally, it was shown that for the vessels with a square base and an radially pumping agitator, the measured Po

number falls between the fully baffled cylindrical vessel and the cylindrical vessels without them [15, 16] with the exact value depending on the positioning of the agitator. In more recent years, several studies were found regarding, for example, mass transfer [17] and blending time [18] or a flow behaviour [19, 20]. However, no large review was found for this geometry.

The use of spherical vessels was discussed in the introduction of the thesis. The largest number of uses of this geometry were found for anaerobic digesters, which are often egg-shaped [21, 5], but the data are generally focused on the underlying biological processes and the mixing equipment is generally tested in a cylindrical vessel. According to Ameur [22], who conducted a comparison study between a flat bottom cylindrical vessel, a dished bottom cylindrical vessel and a spherical vessel, the behaviour of the power number for a radial agitator is similar across the geometries. A similar result to the one found for rectangular vessels. Another such study was carried out by Ammar et al. [23] with a PB6 agitator. An interesting result of this study is that the Po value appears to behave similarly in cylindrical tanks with curved bottoms and in spherical ones. Therefore, an assessment will be made whether similar behaviour can be seen in our results for various agitators. An article regarding the comparison of particle suspension in different geometries was produced by Tacă and Păunescu [24], which concluded that the optimum shape of a vessel is a sphere equipped with baffles. However, compared to the previous two geometries, there seems to be a lack of basic information regarding homogenisation, fluid behaviour, or the performance of common agitators.

It is apparent from this chapter, that for spherical vessels, there is little amount of data available in the literature, as even basic information such as homogenisation times for common agitators was not found. It is therefore the goal of this thesis to measure and evaluate the performance of several different methods of mixing.

### 1.2.2 Mechanical mixing using agitators

Mixing using an agitator is found throughout the process industry and is thus well explored. The types of agitators can be divided according to the rotation speed as slow or rapid, or by the direction of the induced flow as radial, axial, or tangential. This classification is sometimes misleading, as an agitator can induce flow in multiple directions [10]. Baffles are often used in conjunction with rapid impellers because they disrupt the unwanted tangential flow, as it hinders mixing. The added benefit is that the flow is transformed into a more desirable vertical direction [3].

There are hundreds of types of agitators used in the industry. In this thesis, six different agitators were tested, all of which were of the rapid type. From the radial category, RT6 was chosen and from the axial category three hydrofoils FB3, FB6, and A310 were selected. As mixed-flow agitators, PB6 and VJ3 were used.

The frequent use of agitators in the industry is due to their variability. In different configurations, they are suitable for a range of differently sized vessels. They can be applied to facilitate mass or heat transfer, particle suspension, gas dispersion, or emulsion of immiscible fluids [3].

#### *1.2.2.1 Flow in agitated batch*

The Reynolds number Re is defined as the ratio between inertia and viscous forces. As such, it indicates which type of flow is dominant. Generally, two main regions of flow are considered, a creeping flow and a turbulent flow. For mechanically agitated vessels, the creeping flow region is generally when Re < 10, while fully developed turbulent flow occurs when Re > $10^4$ with the transitional region in-between [3]. Mixing is generally performed in the turbulent flow region, as the turbulent mass transfer is superior to pure creeping flow convection, but creeping flow may be preferred when dealing with delicate substances [25]. Because the flow conditions affect the behaviour of other characteristic numbers, the derivation of Re is presented to illustrate where these differences come from.

According to the definition, the Re number originates from the dimensionless analysis of the N-S equation (6). To use the analysis, the variables must be replaced by their dimensionless counterparts defined by equations (9)-(11). The resulting dimensionless form of the N-S equation is shown in equation (12).

$$\vec{u}^* = \frac{\vec{u}}{nd} \tag{9}$$

$$t^* = nt \tag{10}$$

$$\nabla^* = \nabla d \tag{11}$$

$$\frac{D\vec{u}^*}{Dt^*} = -\frac{\nabla^* p}{\rho n^2 d^2} + \frac{\mu}{nd^2\rho}\nabla^{*2}\vec{u}^* \tag{12}$$

From equation (12) a few pieces of information can be extracted. The definition of dimensionless pressure p* for turbulent flow arises from the pressure term and is displayed as equation (14). The fraction before the stress diffusion term defines the Re number for liquids stirred by an agitator and, as such, is presented as equation (13).

However, equation (12) is not valid for Re → 0. This fact disallows its use for the description of creeping flow (Stoke's flow), a dominant type of flow at low values of Re. Continuing the inspection, when Re → ∞, the whole stress diffusion term can be disregarded, hence for the developed turbulent flow, u* and p* are functions of t* and x*.

$$Re = \frac{nd^2\rho}{\mu} \tag{13}$$

$$p_t^* = \frac{p}{\rho n^2 d^2} \tag{14}$$

Adapting equation (6) to accommodate for the low values of Re, equation (15) is obtained. The definition of Re remains the same, however, the pressure term has changed, therefore at low values of Re, p* is defined according to equation (16). Moreover, when Re → 0, the inertia term can be disregarded and as a consequence, u* and p* are only functions of x*.

$$\frac{nd^2\rho}{\mu}\frac{D\vec{u}^*}{Dt^*} = -\frac{\nabla^* p}{\mu n} + \nabla^{*2}\overrightarrow{u^*} \tag{15}$$

$$p_c^* = \frac{p}{\mu n} \tag{16}$$

In summary, the result of this analysis is the confirmation of three different regions of characteristic flow under which the agitated vessel can operate. At Re → 0, the creeping flow is dominant, and the dimensionless pressure and the fluid velocity are functions only of position in the vessel. At higher values of Re, the flow regime begins to change to turbulent and the transition region is entered, where both the dimensionless velocity and pressure become additionally functions of time and the Re itself. However, the dependency on the Re value lessens at its higher values as the stress diffusion term loses on importance and the developed turbulent region is entered. Furthermore, assuming that the flow behaviour repeats periodically, mean values may be used to remove the time dependency from the variables. This conclusion is important as it establishes the regions, which are later used for the assessment of the experiments throughout the thesis.

### *1.2.2.2 Agitator power consumption*

The power number Po is one of the fundamental numbers that describes a system with an agitator, as it enables the estimation of the power draw under working conditions based on previous experience. It is also one of the parameters necessary for a properly executed scale-up [3]. Consequently, understanding where the number comes from and its expected behaviour is necessary for the successful design of an agitated vessel and its proper evaluation in the experimental part.

The power necessary for keeping the agitator rotating at constant speed is equal to the amount of drag affecting the agitator; this relation is expressed by equation (17). In this equation, the force acting on the agitator blade is caused by the drag of the fluid, defined by equation (18) as the impact of the stress tensor (eq.(19)) on the blade surface.

$$P = \iint_{(S_B)} \vec{u} \cdot d\vec{F} \tag{17}$$

$$\vec{F} = \left(\vec{\vec{\sigma}} \cdot \vec{n}\right) dS_B \tag{18}$$

$$\vec{\vec{\sigma}} = -p\vec{\vec{\delta}} + \vec{\vec{\tau}} \tag{19}$$

After substituting equations (5), (18) and (19) into equation (17), a fairly complex equation (20) is formed.

$$P = \iint_{(S_B)} \left(\vec{u} \cdot \left[-p\vec{\vec{\delta}} + 2\mu\overrightarrow{\overrightarrow{\Delta}}\right] \cdot \vec{n}\right) dS_B \tag{20}$$

To enable assessment, it is further modified into its dimensionless format. This transformation utilizes equations (9), (11), (20), and (14) or (16), depending on the type of flow regime, as the power is a function of pressure, and the definition of dimensionless pressure depends on the flow regime. Therefore, the necessary power in the turbulent flow region is described by equation (22) and in the creeping flow region by equation (23).

$$S^* = \frac{S_B}{d^2} \tag{21}$$

$$P = \rho n^3 d^5 \iint_{(S^*)} \left(\vec{u}^* \cdot \left[-p_t^*\vec{\vec{\delta}} + \frac{2}{Re}\overrightarrow{\overrightarrow{\Delta^*}}\right] \cdot \vec{n}\right) dS^* \tag{22}$$

$$P = \mu n^2 d^3 \iint_{(S^*)} \left(\vec{u}^* \cdot \left[-p_c^*\vec{\vec{\delta}} + \overrightarrow{\overrightarrow{\Delta^*}}\right] \cdot \vec{n}\right) dS^* \tag{23}$$

Finally, the power number Po is defined by equation (24) as the dimensionless power for the developed turbulent flow.

$$Po = \frac{P}{\rho n^3 d^5} \tag{24}$$

The relation between Po and Re numbers is illustrated in Fig. 1. For this illustration, the behaviour of the PB6 agitator in a cylindrical vessel with baffles was used [10]. In the creeping flow region, Po is inversely proportional to Re, which can be summarised using equation (25). This conclusion can be reached when the definition of Po is substituted into equation (23).

$$Po \cdot Re = const. \tag{25}$$

On the contrary, in the developed turbulent region, when Re $\rightarrow \infty$, the value of Po is supposed to be constant since the effect of Re is lost due to it being a denominator in equation (22). Therefore, at high values of Re, the Po should adhere to equation (26).

$$Po = const. \tag{26}$$

Such behaviour is similar to that of the drag coefficient, which is not surprising as their origin is similar in nature. These results are important as in chapter 3.2, as they are used to evaluate the measured data.

For the standard set-up of the cylindrical vessel with baffles, with $D/H_2$ and D/d equal to 3. The Po value for the PB6 agitator found in the literature was between 1.65 [26, 3] and 1.7 [27]. The value of 1.7 was used as the reference value in this thesis, as it was obtained with an imprecision in the exact positioning of the agitator in mind.

There are three main methods how to measure power draw [3]. It is possible to use the temperature increase of the fluid, as it should be proportional to the energy dissipated by the agitator. However, this method is considered less ideal as it requires a well-insulated vessel. Moreover, it also disrupts the consistency of the experiment, as with an increase in temperature, the physical properties of the fluid change too. Hence, the most preferred method is the measurement of the reaction torque. The main disadvantage of this method is that other friction loads, such as friction applied by the bearings or the motor, are also measured. This, however, can be overcome by measuring a free-spinning agitator and subtracting the result from the measurement taken under load. Theoretically, the simplest method is to use the motor power, as it does not require any substantial modification of the device, only a suitable wattmeter connected to the motor phases. It is, however, less ideal than the direct measurement of torque as it suffers from the same problems, but it also must incorporate the efficiency curve of the motor to achieve an exact measurement.

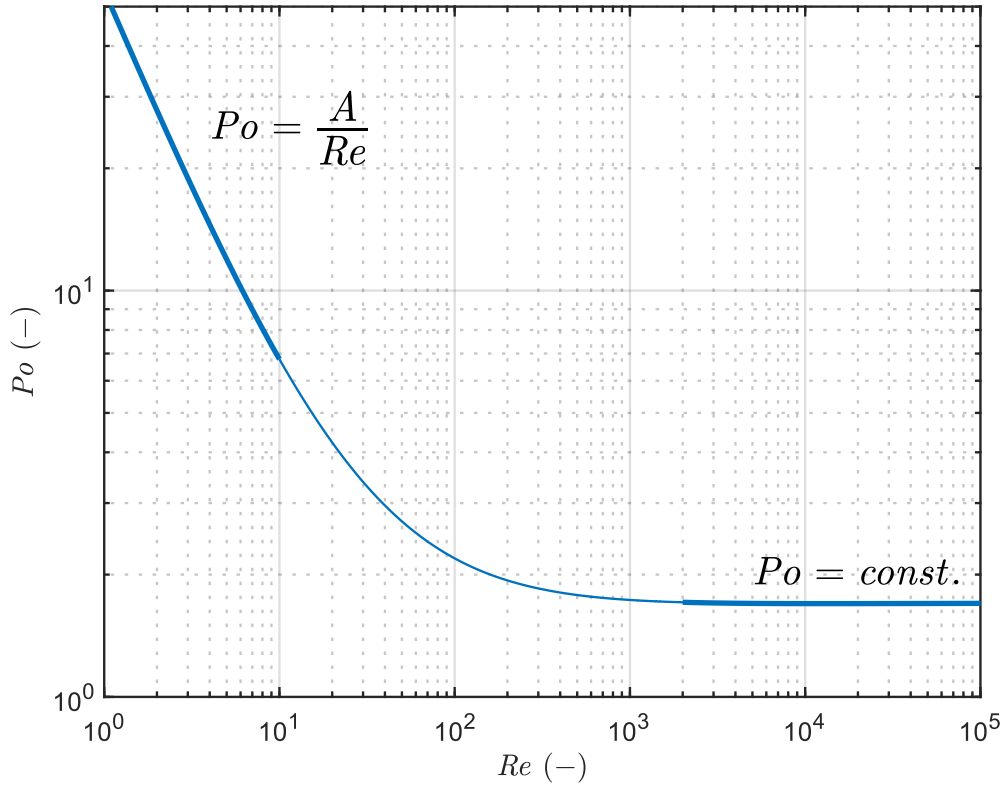


***Fig. 1.*** *Power number as a function of Reynolds number*

### *1.2.2.3 Agitator homogenisation time*

The agitator blending time is the last dimensionless number discussed in this section. It is mainly useful for the calculation of the time necessary to homogenize the vessel. The problem is mainly governed by the transport of mass, which itself is influenced by the convection in the system. This makes the problem more complicated, as it requires solving a more complex set of partial differential equations.

As suggested in the literature [10], the homogenization time may be defined as the time necessary for dimensionless concentration $c_A^*$ to become constant. Using this definition and the information stated in the introductory paragraph, the dimensionless agitator blending time can be derived from the dimensionless analysis of the mass transport equation (8). The conditions under which this equation may be used were presented in chapter 1.1. If the effect of the reaction is not insignificant, a more in-depth analysis is necessary. The definitions (9)-(11) of dimensionless parameters from chapter 1.2.2.1 were used. Additionally, the dimensionless version of $c_A$ was not yet defined; hence it is presented in equation (27). After combining the equations and some restructuring, the final form of the dimensionless mass transfer equation (28) is reached.

$$c_A^* = \frac{c_A - c_A^0}{c_A^f - c_A^0} \tag{27}$$

$$\frac{\partial c_A^*}{\partial t^*} + (\vec{u}^* \cdot \nabla^*) c_A^* = 0 \tag{28}$$

From this equation, the conclusion can be made that the t* is a function of $\vec{u}^*$, $c_A^*$ and x*. Combining this information with the result reached in chapter 1.2.2.1, namely that u* is a function of x* and Re, t* may be expressed as a function (29) of several variables.

$$t^* = f(c_A^*, x^*, Re) \tag{29}$$

Finally, using the definition of homogeneity, we may assume the value of $c_A^*$ to be constant throughout the batch, resulting in t* being only function of Re. Consequently, the three flow regions discovered in chapter 1.2.2.1 are to be expected. For the region of creeping flow, the value of Re $\rightarrow$ 0 and its influence is negligible, hence the outcome formulated by equation (30) is discovered.

$$nt_h = t^* = const. \tag{30}$$

However, in the transition region, t* remains as a function of Re (eq. (31)). This is due to the not insignificant influence of Re on the $\vec{u}^*$.

$$nt_h = t^* = f(Re) \tag{31}$$

In the region of developed turbulent flow, the influence of Re diminishes again. Therefore, the value of t* is again supposed to be constant (eq. (30)). However, the value is different from the one in the creeping flow region.

As a consequence, this outcome allows the assessment of the blending experiments in chapter 3.1.1 as all agitators tested should behave according to this theory, thus allowing for their comparison. The value of $nt_h$ for the PB6 agitator in a cylindrical vessel with baffles (D/d = 3 and $H_2$/d = 1, at 95% homogeneity level), which was found in the literature, is 30.1 [26].

There are several options for how to measure the homogenisation time. Starting from its definition, it is the time necessary for the system to reach homogeneity after a sudden change. The sudden change can be induced by several methods, the simplest of which is to inject a substance into the vessel. The following measurement consists of monitoring the concentration value of a given substance throughout the vessel and waiting until it appears to settle around a constant value. The concentration can be measured using the conductivity of the fluid [3]. As the method requires the fluid to be conductive, the added liquid should be an electrolyte. The main benefit of this method is that it enables real-time measurement of concentration without the interference of the human factor.

Therefore, the measurement is more precise compared to the second method. However, the method requires the installation of probes, which can affect the local mixing and offer only localized information about the state of the batch. Prior knowledge about the mixing process is therefore required to place the probes properly.

For this purpose, the so-called Colorimetric method [3], based on the visualization of the homogenization process either by adding a colourant or using a chemical reaction, is used. The decolorization process achieved by chemical reaction is preferred, as it enables the identification of the last pocket of unhomogenised fluid, which may be overlooked when using a dye. Several different chemical reactions can be used for this purpose, the most common one being Acid-Base with indicator. As the name suggests, the method utilizes a change in pH that influences the colour of an indicator. The added benefit of this method is that it also visualizes the flow within the batch. However, although easy to set up and perform, the method is inherently imprecise as it depends on the subjective view of the one performing the experiment and may therefore vary in strictness. A recorder of sorts should always be used to allow for revaluation of the results. Other methods such as temperature measurement or changes in optical properties may also be used [3].

### 1.2.3 Hydraulic mixing

Using a liquid jet to mix a batch was first explored by Fossett and Prosser [28], where they illustrated the usefulness of this method of mixing in a large chemical reactor and in a swimming pool. A general overview of this method may be found in the Mixing in the process industry [29] edited by Harnby et al. In this publication they summarize that jet-induced mixing is suitable for large vessels, where several agitators would be necessary to provide mixing. The greatest added benefit of using jet-style mixing is the absence of moving parts in the batch [30]. The downside is the higher energy consumption, which is approximately seven times higher than the energy used by an agitator if the same homogenization time is to be reached [29].

The jet mixing appears to utilize four main methods to achieve mixing; bulk transport of jet liquid from the nozzle toward remote areas, bulk transport induced in remote areas, bulk transport induced by entrainment of liquid into the jet stream and by turbulent mixing of fluids on the jet boundary [29].

The effectiveness of the jet-induced mixing is largely dependent on the positioning of the nozzle. Wall-mounted nozzles are commonly used in the literature with horizontal or inclined positioning [30].

### *1.2.3.1 Flow in a jet agitated batch*

Similarly to the method used in chapter 1.2.2.1 a dimensionless analysis of the Navier-Stokes equation may be applied to the problem of jet-induced mixing. However, compared to the system utilizing an agitator, a system with a jet can be approached from two different angles. The first option is to utilize the theory developed for the pipe flow and describe the turbulence in the system using the flow properties at the jet nozzle. In such a case, the value of Re would be defined by equation (32).

$$Re_p = \frac{\bar{u} d \rho}{\mu} \tag{32}$$

The other option is to base the system around the vessel. Such a method was used, for example, by Maruyama et al. [31]. For this, however, new dimensionless variables must be defined, as the ones used in 1.2.2.1 were defined with an agitator in mind. Therefore, new dimensionless definitions (33)-(35) were created. Substituting into the N-S equation (6), a new dimensionless variant (36), describing the flow induced by the jet stream, is created.

$$\vec{u}_V^* = \frac{\vec{u}}{\bar{u}} \sim \vec{u} \frac{\dot{V}}{d^2} \tag{33}$$

$$t_V^* = \frac{t}{MRT} = t_h \frac{\dot{V}}{V} \sim t_h \frac{\dot{V}}{D^3} \tag{34}$$

$$\nabla^* = \nabla \mathrm{D} \tag{35}$$

$$\frac{D\vec{u}_V^*}{Dt_p^*} = -\frac{d^2 D^2 \nabla^* p}{\rho \dot{V}} + \frac{\mu D}{\rho \dot{V}} \nabla^{*2} \vec{u}_V^* \tag{36}$$

From this equation a new definition (37) of the vessel Reynolds number arises, with properties similar to its agitator equivalent. Using a similar procedure, the same two expected extremes of flow behaviour are found with a transition region in between.

$$Re_V = \frac{\rho \dot{V}}{\mu D} \tag{37}$$

### *1.2.3.2 Jet homogenisation time*

The result of the homogenisation process is the same whether it is achieved by an agitator or a jet; therefore, the same methods of measurement and evaluation may be used as the ones described in chapter 1.2.2.3. When it comes to jet-style homogenisation, several different correlations were found in the literature. The first theory describing mixing in tanks using a jet was formed by Fosset and Prosser in their work The Application of Free Jets [28], arising from their work on oil storage tanks. The conclusion of their work is equation (38).

$$t_p^* = \frac{t_h}{t} = t_h \cdot \frac{\sqrt{\dot{V}\bar{u}}}{D^2} \sim t_h \cdot \frac{\bar{u}d}{D^2} \tag{38}$$

They derived this equation using the law of conservation of momentum for an incompressible flow (eq. (39)) applied to the injected fluid. They reasoned that the momentum at the jet nozzle must be equal to the momentum of the induced stream with cross section $S_j$ and velocity v inside the vessel. The time necessary for the stream to traverse the vessel is then proportional to the characteristic length of the vessel (eq. (40)). Combining these two equations and supposing that $S_j \sim D^2$ and $L \sim D$, we obtain equation (38).

$$\dot{V}\bar{u} = S_j \bar{v}^2 \tag{39}$$

$$t = \frac{L}{\bar{v}} \tag{40}$$

As the behaviour of the fluid inside of the vessel is described using the jet stream, the pipe Re number at the jet nozzle (eq. (32)) was used to describe the flow. In the following years, several different authors improved the theory by adding correlations for different angles and positions of the nozzle [32]. However, based on the results published in the aforementioned work, it is apparent that no overarching conclusion, similar to the one reached in chapter 1.2.2.3, can be made, only that the result should be a function of $Re_p$ (eq. (41)).

$$t_h \frac{\bar{u}d}{D^2} = t_p^* = f\left(Re_p\right) \tag{41}$$

There is, however, another way to assess the jet-induced flow. Using a similar approach to the one used on agitators described in chapter 1.2.2.3 and utilizing the groundwork laid down in the previous chapter, a result similar to that of Maruyama et al. published in their work Jet mixing of fluids in tanks [31], is obtained. Similarly to the derivation of the vessel Reynolds number, the dimensionless variables defined by equations (33)-(35), were applied to the mass transport equation (8). As in chapter 1.2.2.3, if a slow chemical reaction is present, the simplified version of the equation is not valid, and a more thorough analysis is necessary. The definition of $c_A^*$ remains the same, hence equation (27) was reused. After some restructuring, a dimensionless form of the mass transport equation (42) is formed.

$$\frac{\partial c_A^*}{\partial t_V^*} + \left(\frac{D}{d}\right)^2 (\vec{u}^* \cdot \nabla^*) c_A^* = 0 \tag{42}$$

By analysing the equation and combining its result with the information gained from the derivation of Re, the information that $t_V^*$ is a function of several different parameters (eq. (43)) is obtained. This relation is similar to the one reached in 1.2.2.3, differing only in its dependence on the D/d fraction.

$$t_V^* = f\left(c_A^*, x^*, Re_V, \frac{D}{d}\right) \tag{43}$$

Therefore, the expected outcome should not be dissimilar to the one expected from the agitators. The only difference is the exact values of $t_V^*$ due to different definitions. Consequently, in the creeping flow region, the $t_V^*$ should be constant (eq. (44)).

$$t_h \frac{\dot{V}}{D^3} = t_V^* = const. \tag{44}$$

In the transition region, it should remain a function of $Re_V$ (eq. (45)).

$$t_h \frac{\dot{V}}{D^3} = t_V^* = f(Re_V) \tag{45}$$

And in the region of developed turbulent flow, a constant value (eq. (44)), but different from the one in the creeping flow region, should be reached.

As there seem to be two competing theories on how to describe the homogenisation induced by a jet, as part of this thesis, experiments were conducted to assess which of them is more suitable for the spherical vessel.

### 1.2.4 Pneumatic mixing

Unfortunately, little information has been published in the literature on the topic of batch mixing using a pneumatic system. Neither Perry's chemical engineers' handbook [33] nor the Industrial Mixing Handbook [3] provide substantial information on mixing in a sparged system without agitation. The information published on gas-liquid systems generally focuses on mass or heat transfer. Mixing caused by the bubbles is often mentioned as a side note, as it may affect mixing on a microscale, but if homogenisation is necessary, an agitator should be used.

Unagitated sparged systems may be found in water treatment plants [11]. In these plants, it is often utilized in activated sludge systems, where it is mainly used to supply oxygen to the bacteria. It also has the effect of mixing the liquid and suspending the sludge, but those are secondary benefits of the method. The system is also found in various flotation units.

# 2 Experimental measurements

As there is a small amount of data available in the literature on the topic of spherical vessels, several experiments were conducted. These experiments are divided into three categories. Those categories are the measurements of blending time, power consumption, and suspension of particles using an agitator.

All the experiments were carried out in the same spherical vessel with an inner diameter D of 320 mm and a flat bottom base. The sketch of the vessel can be seen in Fig. 2. The exact setup for each series of experiments is presented in the corresponding chapter. All the experiments were carried out with 13 L of tap water. Therefore, the exact height of the water surface depended on the experimental setup but did not vary significantly. The initial value of H was 215 mm. The total height of the vessel $H_s$ was 270 mm, the diameter of the top opening $D_t$ was 206 mm, and the diameter of the base $D_b$ was 125 mm. All measurements were taken using a ruler.

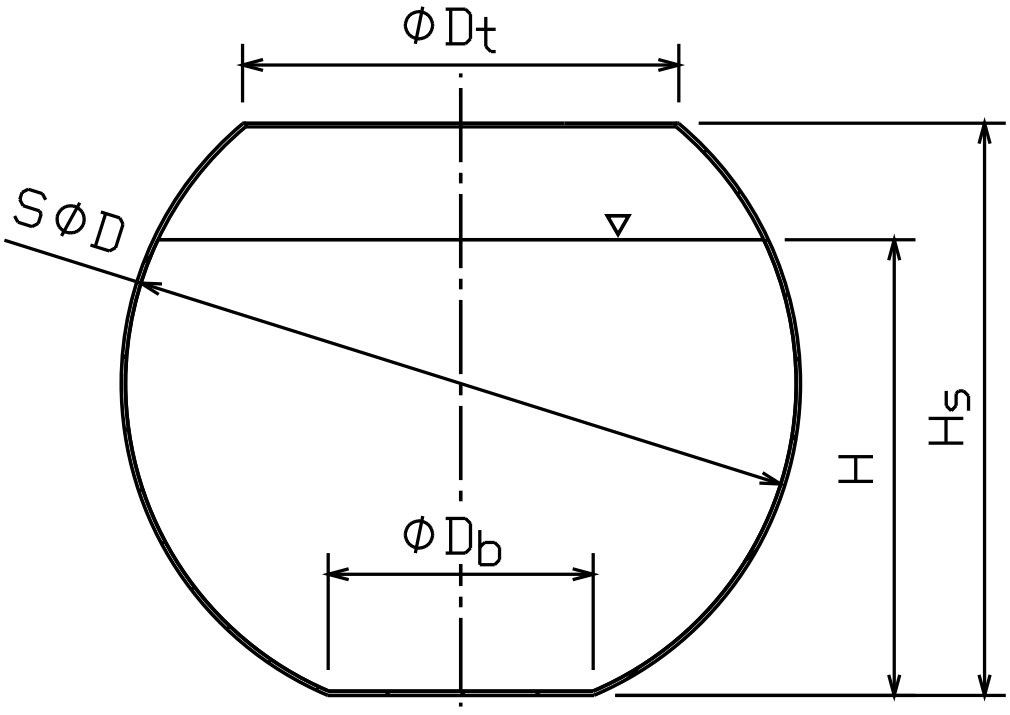


***Fig. 2.*** *Sketch of the **s**pherical vessel used in the experiments*

To assess which agitator type is the most suitable for mixing in spherical vessels, several different agitators with different pumping directions, given by their geometry, were tested. As the nomenclature differs between nations, a series of agitator pictures with the corresponding abbreviations used in this thesis is presented in Fig. 3. Additional information about the geometry of the agitators, such as diameter, angle of blades, or a trademarked name are presented in Tab. 1.

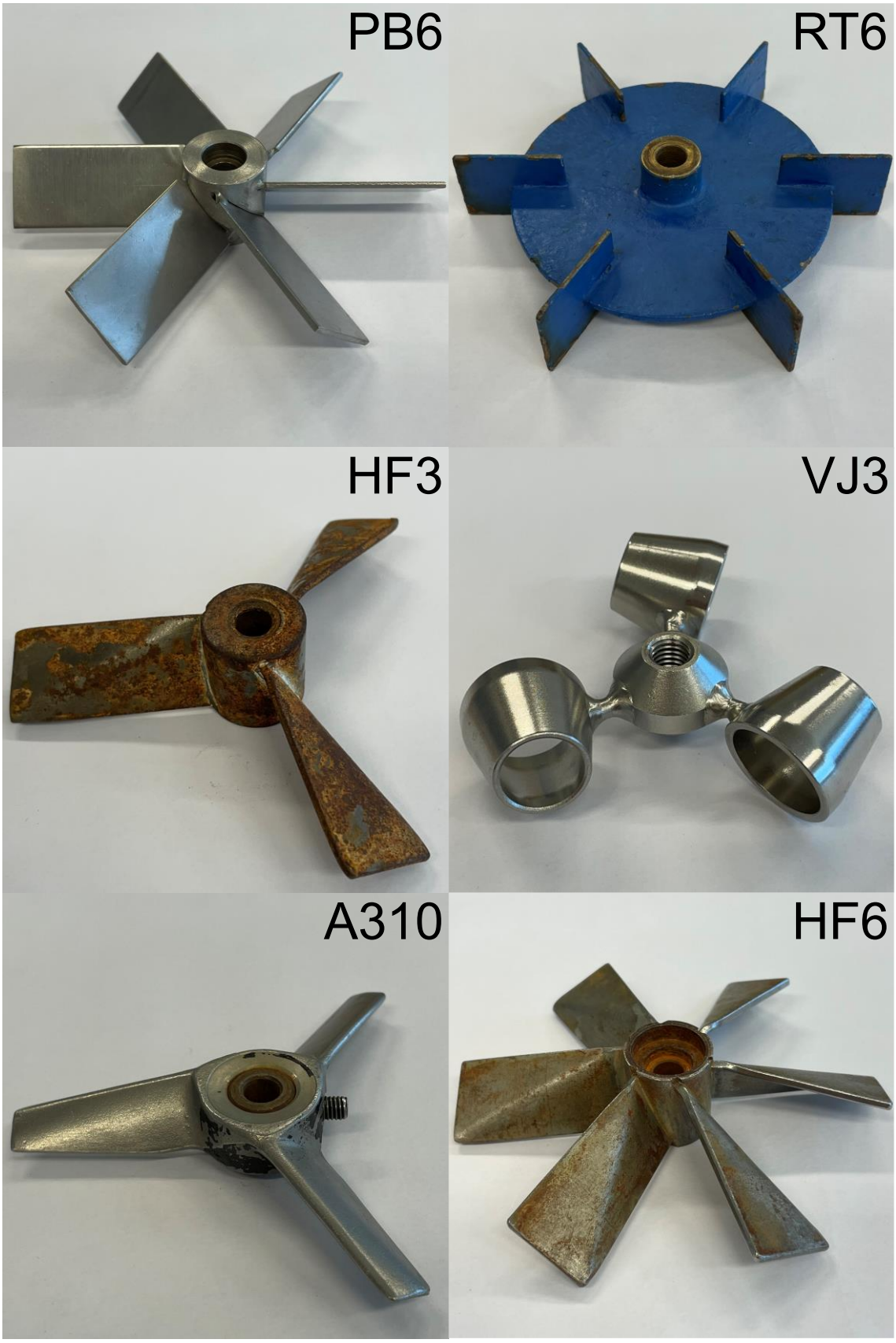


***Fig. 3.*** *Agitator types with the nomenclature used in this thesis*

***Tab. 1.*** *Geometrical parameters of the used agitators*

| *Abrv.* | *Diameter (mm)* | *Number of blades* | *Angle of the blades* | *Direction of pumping* | *Trademarked name* |
|---|---|---|---|---|---|
| *PB6* | 100 | 6 | 45 | Axial | |
| *RT6* | 100 | 6 | 90 | Radial | |
| *FB3* | 100 | 3 | 67 – 25 diagonally folded | Axial - hydrofoil | |
| *FB6* | 100 | 3 | 67 – 25 diagonally folded | Axial - hydrofoil | |
| *VJ3* | 100 | 3 | - | Radial | Visco Jet |
| *A310* | 100 | 3 | - | Axial - hydrofoil | Lightnin |

## 2.1 Blending experiments

To measure the homogenisation time, the Acid-Based indicator method was used. The method was chosen because of its ability to visualize the flow inside the batch. This was important because there was no prior knowledge of how the mixed liquid is going to behave. Solutions of 1 M $H_2SO_4$ and 1 M NaOH were prepared in advance using laboratory scales (precision ±0.001 g), a 1 L graduated cylinder, and a pipet. As an indicator, a 1 % phenolphthalein solution was used.

An analysis of the reaction had to be made to check, whether it influences the blending time as was discussed in chapter 1.1. For this reason, the Da number was calculated according to equation (7). Unfortunately, the precise value of the kinetic constant $k_r$ for this exact reaction was not found in the literature; therefore it was approximated at $10^{11}$ L/(mol.s) using the known values of reactions similar in nature, published in [34] or found in the NIST database [35]. The mixing time used in the calculation was 5 s, chosen as the shortest measurement time in the experimental part. The computed Da is around $10^{11}$, far greater than the limiting 100, meaning that the influence of the reaction is insignificant, and the theory described in 1.2.2.3 and 1.2.3.2 may be used.

At the beginning of the experiments, several millilitres of phenolphthalein solution were added. The indicator turns pink when the environment is alkaline and colourless when neutral or slightly acidic. The dosage of the solutions used in the experiments was 4 ml of NaOH solution and 2.1 ml of $H_2SO_4$, a 10 ml syringe with 0.5 ml grading was chosen for the addition of chemicals, as its larger diameter allowed shorter piston travel, resulting in more consistent injections. A slightly above stoichiometric ratio was chosen

because of the consistency of the experiments, as with an exact ratio, full decolourization of the liquid was sometimes not achieved. After each measurement, an additional small amount of NaOH solution was added, until the liquid started to become pinkish, therefore neutralizing the overdose of $H_2SO_4$. The experiments were fully recorded with a camera, and the blending time was determined from the footage. The initial time was chosen as the end of the injection of the acid solution, and the end time as the moment when the liquid turned to its original colour in its whole volume. The time difference was set as the difference between the timestamps in the video. The precision of the method varied significantly between sets, but on average the difference between the values in one set of measurements was around ± 2.5 s. However, this time does not incorporate the subjective view of the author and different results would be reached by a different experimenter.

### 2.1.1 Agitator blending

The experiment consisted of an agitator with an adjustable revolution speed. Its shaft was centred to the centre of the top opening using a ruler. The distance $H_2$ between the bottom of the agitator and the base of the vessel was 0.75·d. In the case of VJ3, the distance between the centre of the suction inlet and the base was measured. The setup is presented in Fig. 4. In all experiments, the agitators of axial type were setup to pump downwards.

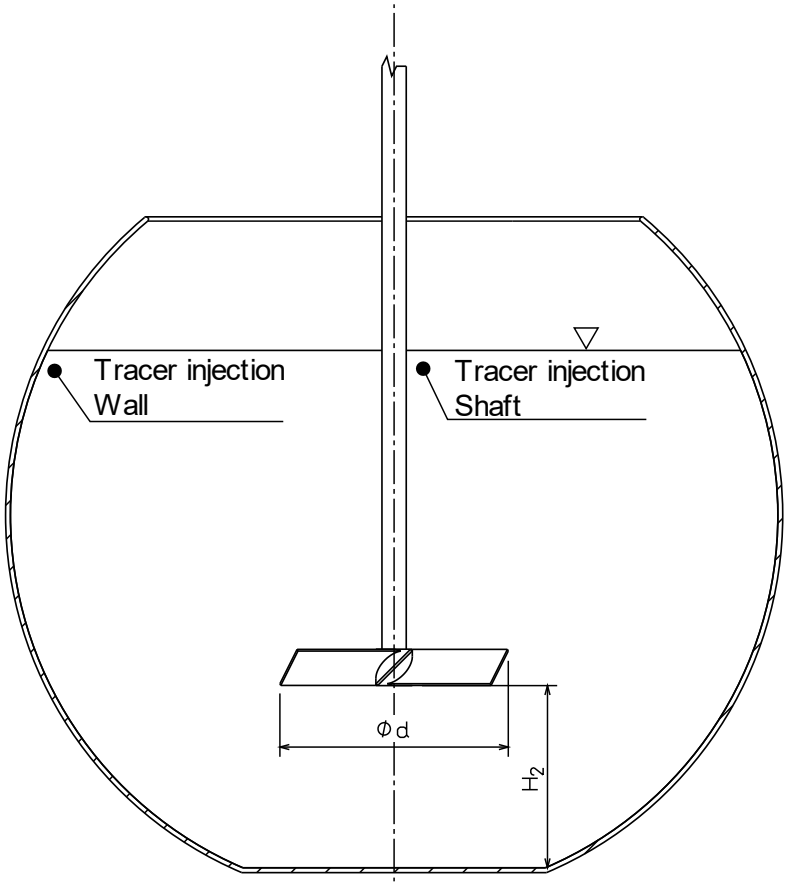


***Fig. 4.*** *Setup of agitator blending*

The measurement was carried out for five different types of agitators, namely, PB6, RT6, FB6, VJ3, and A310. The diameter of the agitators PB6, RT6, FB6, and A310 was 100 mm. The diameter of VJ3 was 60 mm. It was set as the double of the distance between the axis of the shaft and the centre of the suction inlet of the agitator. The experiments were conducted at several different RPMs. The RPM value was gradually increased with around 25 RPM increments until suction of air into the agitator area occurred or the rotation speed was deemed too high. The precision of the RPM control unit was about 2 RPM. To assess the worst-case scenario of injection, two extremes were chosen, injection next to the shaft and injection next to the wall. For each position and RPM setting, the experiment was repeated four times. The injection assessment was performed only on agitators PB6 and RR6, as at high RPM a large vortex began to form, making the measurement inconsistent, as the injection place was a centimetre above the agitator and did not correspond to its original placement.

Lastly, a control measurement was performed on a cylindrical vessel with four baffles, with a diameter D = 300 mm, with the same PB6 agitator. Both $H_2/d$ and H/D used during the experiment were 1. The experiment was conducted to enable the comparison of the gained results with the result found in the literature. The cylinder setup is presented in Fig. 5.

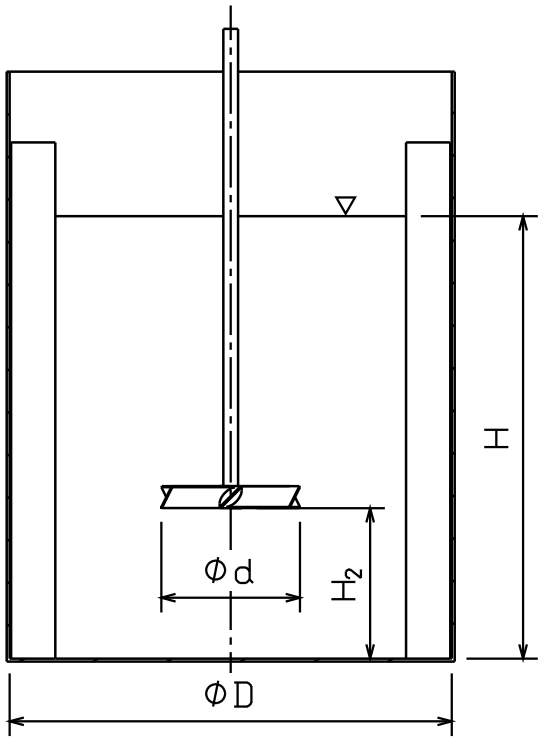


***Fig. 5****. Sketch of the standard configuration calibration vessel with baffles and PB6 agitator*

To illustrate the experiment, four pictures are presented in Fig. 6. This sequence of pictures starts on the left with the injection moment and ends on the right with a fully homogenized batch.

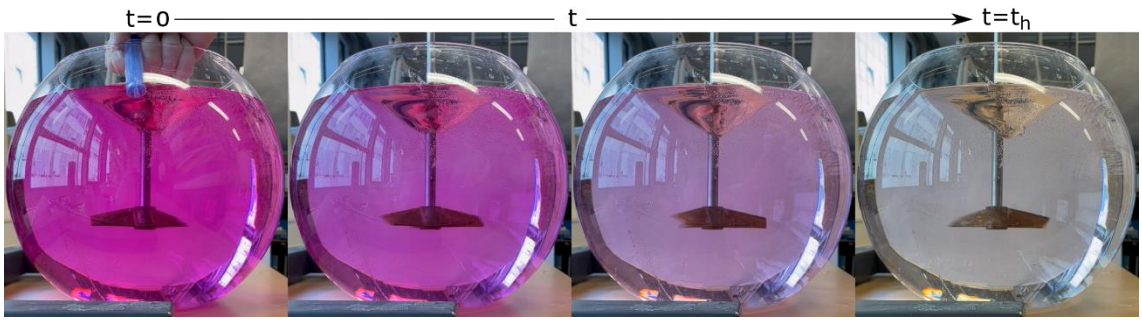


***Fig. 6.*** *Illustration of blending using FB3 at 225 RPM*

### 2.1.2 Jet blending

The creation of a jet nozzle was carried out by gluing an outlet pipe to the bottom of the vessel. The inlet pipe was glued 15 mm beneath the water surface. The pumping was carried out with a peristaltic pump with variable rotation speed. Volumetric flow was measured after every change in pump speed using a stopwatch and a 1 L graduated cylinder. Three main configurations of the input-output positions were tried. Specifically, a tangential outlet configuration with an inlet placed on the opposite side (Tangential outlet), a radial outlet configuration with an inlet offset by 90° to the outlet position (Radial outlet), and an axial configuration with an outlet in the axis of the vessel aimed towards the surface and inlet at the wall. The setups are displayed in Fig. 7, only the endings of the pipes are shown in the figure. The chemicals were injected next to the wall, always on the opposite side to the inlet, the exact positioning is also illustrated in the figure. Additionally, the injections at the centre were tested during the tangential configuration to assess which injection site is worse. The experiment was repeated four times for each position and volumetric flow.

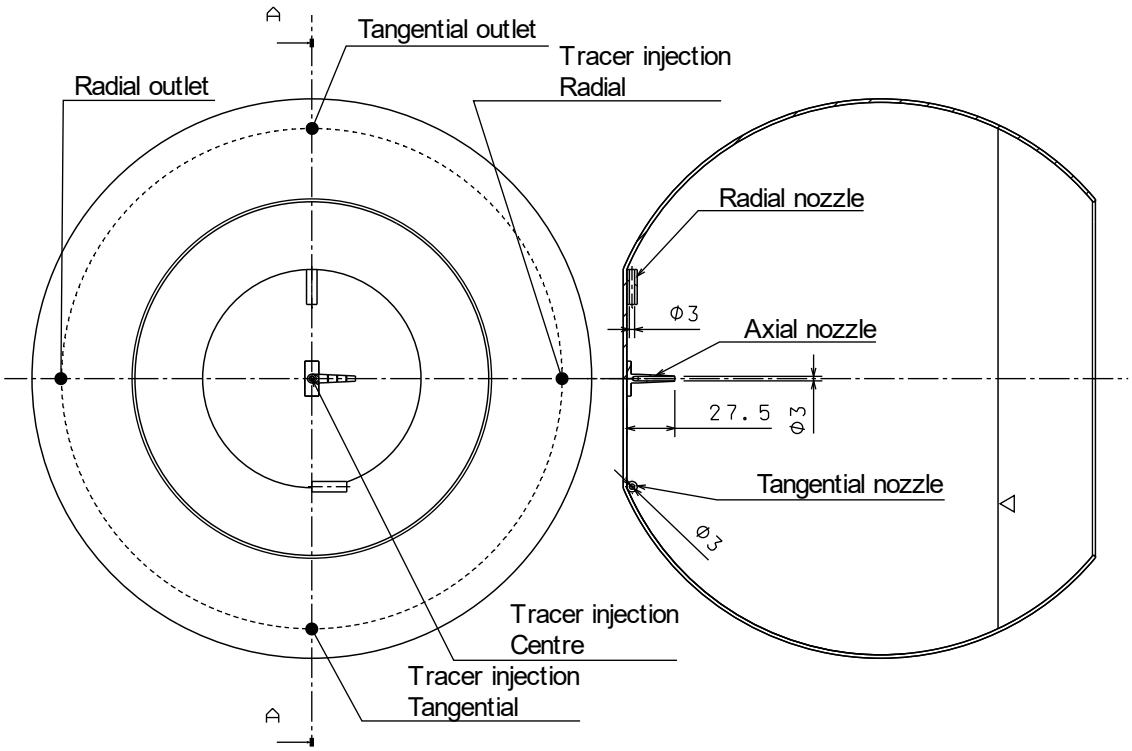


***Fig. 7.*** *Sketch of jet blending setup*

The blending effect of the axially placed jet is illustrated in Fig. 8. This sequence of pictures again starts on the left with the moment of injection and ends on the right with a fully homogenized batch.

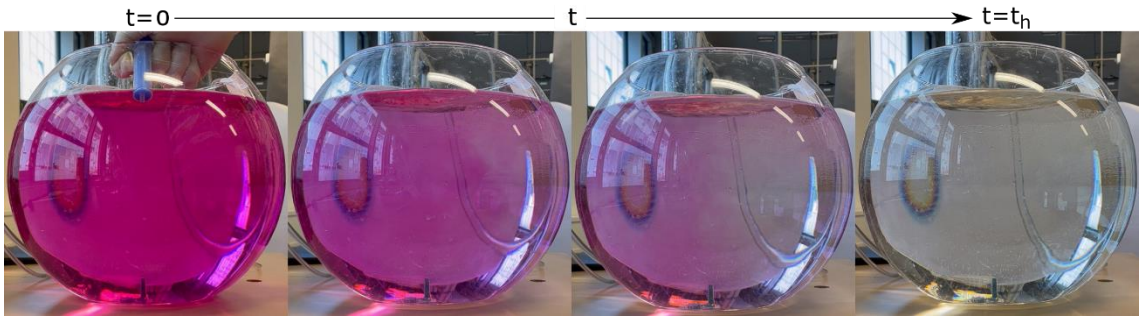


***Fig. 8.*** *Illustration of axial jet blending at a jet velocity of 1.6 m/s*

### 2.1.3 Sparger blending

The bubbles used for the pneumatic blending were created using a torus sparger placed on the bottom of the vessel; the setup can be seen in Fig. 9. The diameter of the torus was 80 mm, and it was placed 25 mm above the bottom of the vessel. The gas was pumped through 16 holes with a diameter of 1 mm. Compressed air was taken from a central distribution system. The pressure was controlled using the inlet reduction valve to 200 kPa (g). Volumetric flow was controlled using a reduction valve integrated with the flowmeter unit. A floating element gas flow meter was used to measure the volumetric flow with a maximal flow of 2100 L/hour, the graduation of the flowmeter was per 70 L/hour. The pressure loss on the sparger was measured using a U-style manometer with a 1 mm graduation. The measurement was repeated four times for each volumetric flow. No worst-case scenario assessment was performed for this setup, as the flow was primarily axial, with the main upward flow rising through the centre and then dispersing towards the walls, hence the acid solution was injected only next to the wall where the flow was the slowest and the least turbulent.

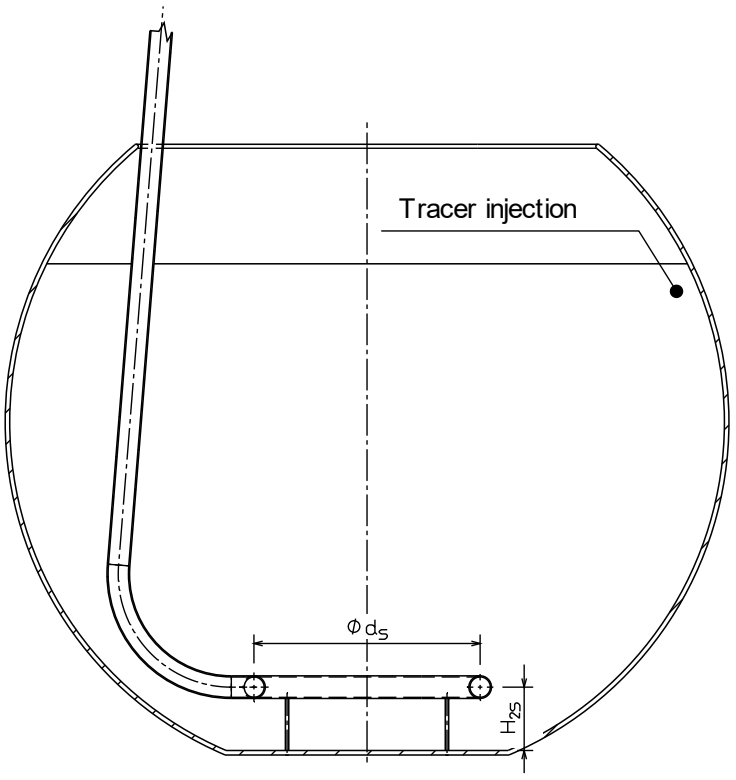


***Fig. 9.*** *Sketch of sparger unit setup*

The blending effect of the sparger unit is illustrated in Fig. 10. This sequence of pictures again starts on the left with the moment of injection and ends on the right with a fully homogenized batch. In Fig. 11. a schematic of the experiment setup with the positioning of the valves and the point of pressure measurement is shown. The length of the pipe between the point of pressure measurement and the torus was approximately 3 m. The inner diameter of the pipe was about 1 cm, and the pipe was made from soft PVC.

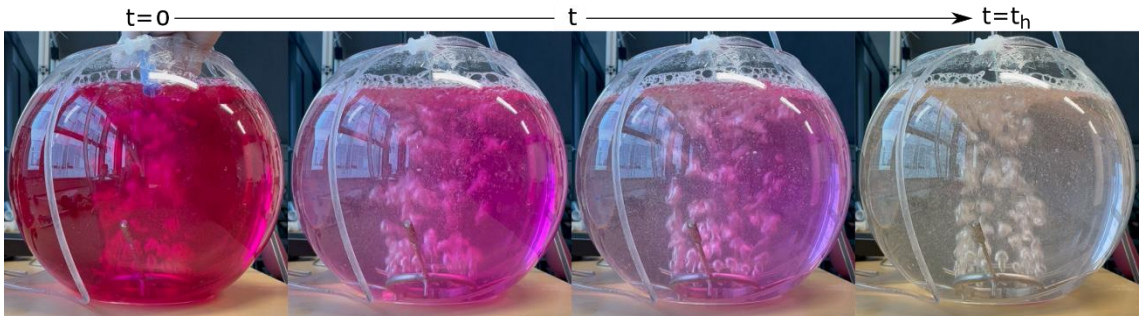


***Fig. 10.*** *Illustration of the sparger blending at a gas volumetric flow of 10.5 $m^3/s$*

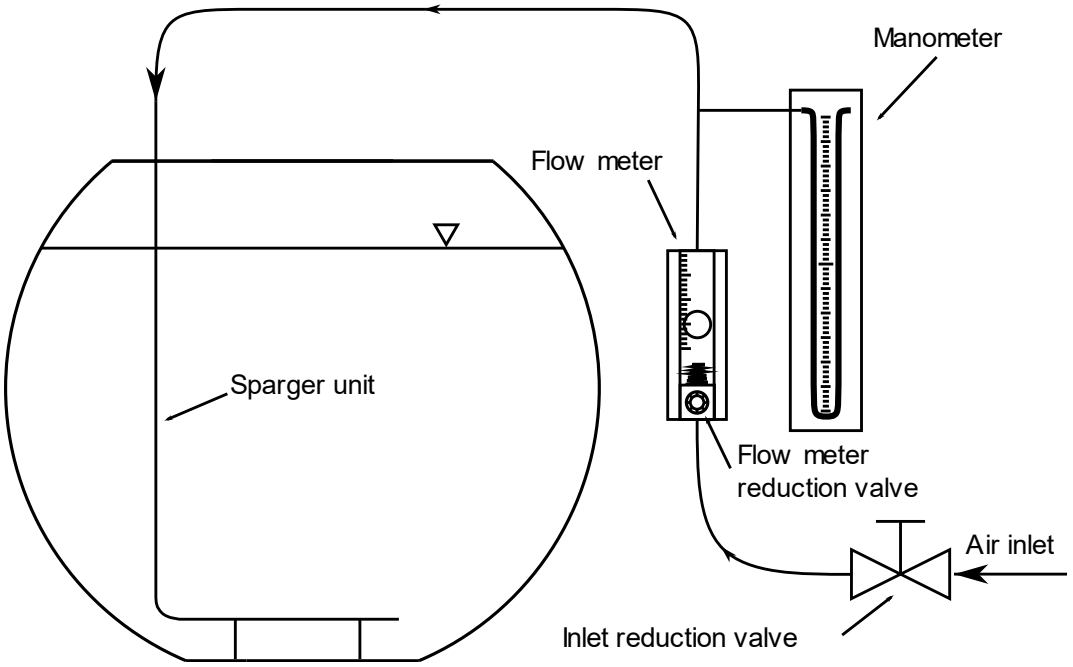


***Fig. 11.*** *Setup of sparger experiment*

## 2.2 Measurement of agitator power input

The experiment setup was like the one seen in Fig. 4. In these experiments, two agitator positions were used, specifically $H_2/d = 0.5$ and $H_2/d = 0.75$, because of the other two experiments. The amount of power put into the system by the agitator was measured using a torque sensor (precision ± 0.5 Nm) and a tachometer attached to the shaft of the agitator. The data were gathered using PLC and interpreted using an Excel script. The RPM value was displayed on the control panel, but the torque value had to be converted from the electric potential difference measured on the sensor. The rotation was slowly increased by 25 RPM increments until suction occurred. The RPM value oscillated about 2 RPM around the set value. The measurement of torque value consisted of 400 values taken for 10 s. To determine the drag from other mechanical parts, a torque value for the free-spinning agitator was also measured at each RPM. The measurement was carried out for all agitator types. The conversion constant was calibrated using a known power number – geometry – agitator setup.

The calibration was performed on a cylinder with four baffles with the PB6 agitator. The diameter of the cylinder was 300 mm, with H/D = 1. The diameter of the agitator was 100 mm with $H_2/d = 1$. The configuration is illustrated in Fig. 5. The agitator shaft was centred to the top opening using a ruler. The diameter of the vessel and the distance of the agitator blade from the bottom were also measured using a ruler. The variant without baffles was also tested. Unfortunately, at around 200 RPM the system hit its resonant frequency; hence, the error of measurement at this value was around 150% for some configurations.

## 2.3 Particle suspension

The ability of the agitators to achieve just suspended state was also tested. The agitators used for this set of experiments were PB6, RT6, FB3, A310, and FB6. The positioning of the agitator was similar to the one presented in Fig. 4 with $H_2/d$ being 0.5. 13 L of water were added to the spherical vessel at the beginning of the experiment. Glass beads were used as the particles of choice with an average diameter of 1 ~ 1.3 mm and a density of 2600 kg/m$^3$. The weight of beads added to the system was measured using scales (precision ± 0.1 g), and the added weight was set as an average of four measurements. The beads were added incrementally and after each addition, all still suitable agitator types were tested. The RPM value was gradually increased until the suspension of all particles was achieved. This state was defined according to the modified Zwietering criteria [36], which means that no particle was stationary for more than 3 s. A visual inspection was used to determine whether all particles are being suspended, the most scrutinized location being the bottom edge of the vessel. When the agitator was not able to achieve suspension, it was removed from the measurement and was not used during subsequent experiments. After the suspension was achieved, the just-suspended rotation speed and height of the suspension layer were noted. The height of the layer was measured using a ruler with a precision about 0.5 cm. When the height of the particle cloud was not constant, a mean value was estimated. Subsequently, the RPM value was again incrementally raised until full blending or suction to the agitator area occurred. To illustrate the measured parameters, Fig. 12 is presented.

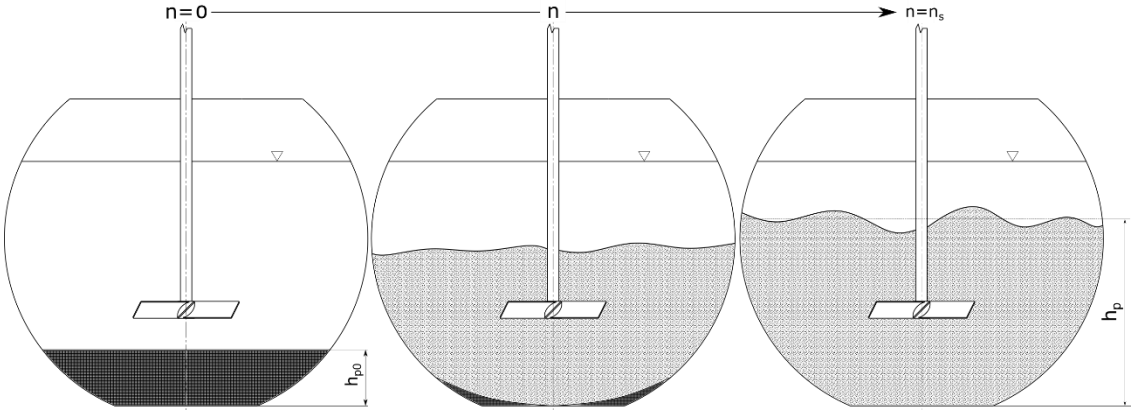


***Fig. 12.*** *Parameters of the particle suspension experiment*

# 3 Experiment results

As mentioned in the previous chapter, several experiments were conducted to evaluate the performance of different types of mixing devices. In this chapter, the results gathered from the experiments and the methods of their assessment are presented. For this purpose, a power function was used as the regression model, with a T-test applied to discern whether the regression parameters have significant influence over its behaviour or if they can be disregarded. The value of parameters was determined using the least-squared method implemented in MATLAB fit function from the Curve fitting toolbox. The regions were created manually using a visual assessment of the measured data and in accordance with the expected behaviour discussed in the previous chapters. For all approximations, Student's confidential intervals were calculated.

## 3.1 Results of blending experiments

### 3.1.1 Results of agitator blending

The data gathered from the experiments described in chapter 2.1.1 were analysed using the theory discussed in chapter 1.2.2.3. The time necessary to homogenize the batch was converted using equation (10) and was plotted in a graph as a function of the agitator Reynolds number defined by equation (13). Three distinguishable regions should appear according to the theory discussed in chapter 1.2.2.3. For low values of Re, the blending is performed under the creeping flow conditions described by equation (30). On the other extreme, at high values of Re, the value should also be constant but with a different value. The transition region is placed between these extremes. In this region, the dimensionless time remains as a function of Re (eq. (31)). As the measured interval is rather small, a simple power function (46) was chosen as it can describe both extremes and should be sufficient for the description of the transition region. The T-test was applied to the regression to determine whether the B parameter significantly influences the regression. When it was deemed unnecessary, the approximation using the mean value was used instead. An overview of the regression parameters and the intervals of Re on which they are valid, are presented in Tab. 2.

$$nt_B = \frac{A}{Re^B} \tag{46}$$

To test the precision of the method, the first set of experiments carried out was the measurement of blending time in a cylindrical vessel using the PB6 agitator. For the geometry with baffles, the value of dimensionless time found in the literature was 30.1 [26]. The graphical representation of the data is presented in Fig. 13.

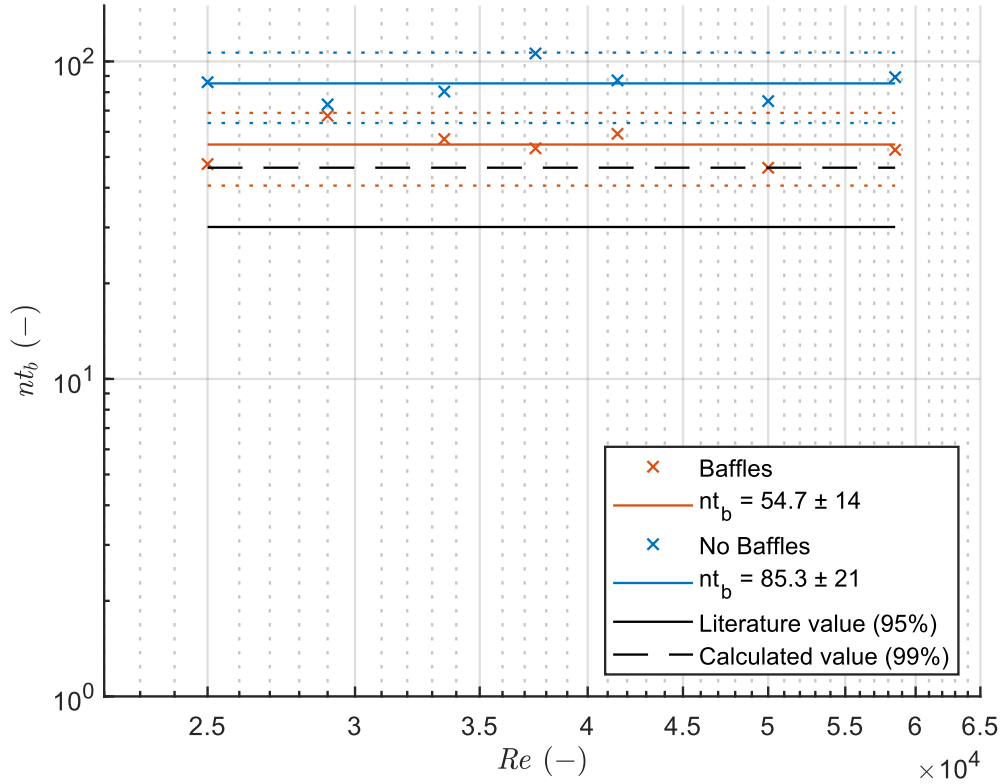


***Fig. 13.*** *Blending using agitator PB6 in a cylindrical vessel*

It is apparent, that the 95 % homogeneity value found in the literature is significantly lower than the one experimentally measured. However, since the method of measurement utilized probes, the assumption can be made that the visual evaluation was far stricter, as the decolouration in the whole volume was set as the point of reference. Equation (47) was provided by Fořt et al. [26], to recalculate the result for stricter homogeneity conditions. For 99 % homogeneity, the value of nt is 46.3, which is high enough to be inside the confidential interval. This result is sufficiently good to continue with the experiments as the imprecision and added strictness are caused by the subjective nature of the method and the limited amount of data. For design purposes, the measurement should be repeated utilizing a more precise method of measurement.

$$(nt_B)_A = (nt_B)_{0.95}\left[\frac{ln(1-A)}{ln(1-0.95)}\right] \tag{47}$$

Subsequently, a set of experiments was carried out on the spherical vessel. The results of the measurement with appropriate confidential intervals for different agitator types are presented in Fig. 14. For the initial two agitators, the influence of injection position was measured, but due to the formation of a large axial vortex and the inherent incapability to maintain a constant place of injection, it was dropped for the remaining experiments. However, the results are presented to illustrate the effect.

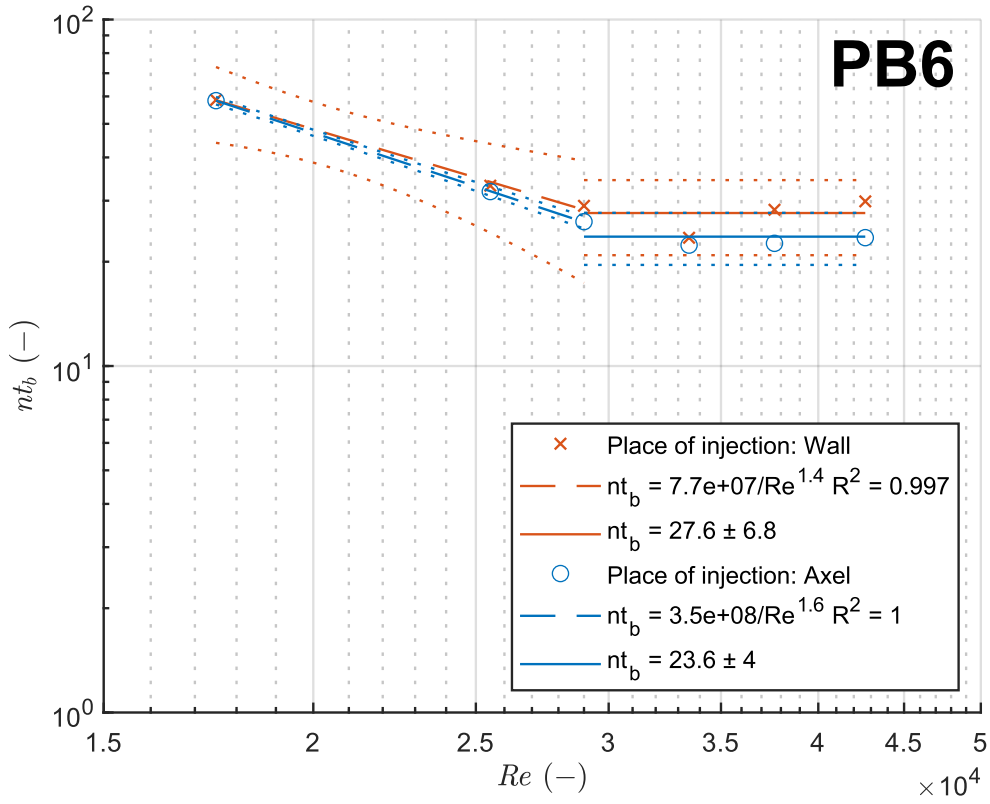
PB6
$10^2$
$10^1$
$10^0$
$nt_b$ (−)
1.5
2
2.5
3
3.5
4
4.5
5
$Re$ (−)
$\times 10^4$
Place of injection: Wall
nt$_b$ = 7.7e+07/Re$^{1.4}$ R$^2$ = 0.997
nt$_b$ = 27.6 ± 6.8
Place of injection: Axel
nt$_b$ = 3.5e+08/Re$^{1.6}$ R$^2$ = 1
nt$_b$ = 23.6 ± 4

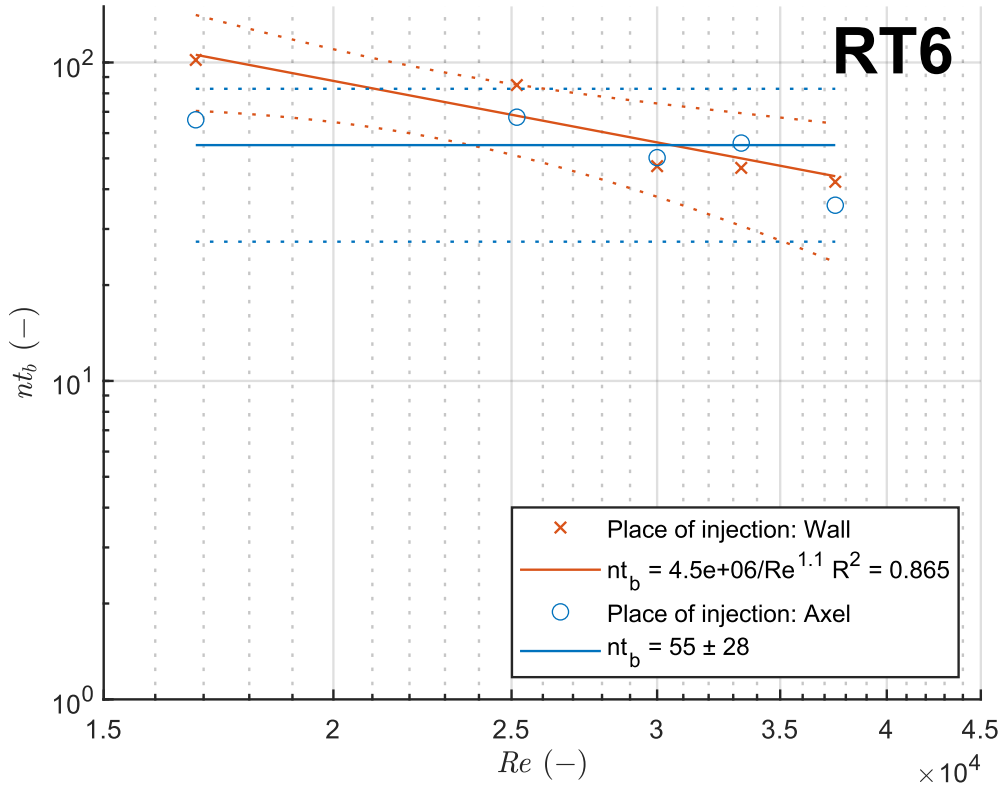
RT6
$10^2$
$10^1$
$10^0$
$nt_b$ (−)
1.5
2
2.5
3
3.5
4
4.5
$Re$ (−)
$\times 10^4$
Place of injection: Wall
nt$_b$ = 4.5e+06/Re$^{1.1}$ R$^2$ = 0.865
Place of injection: Axel
nt$_b$ = 55 ± 28

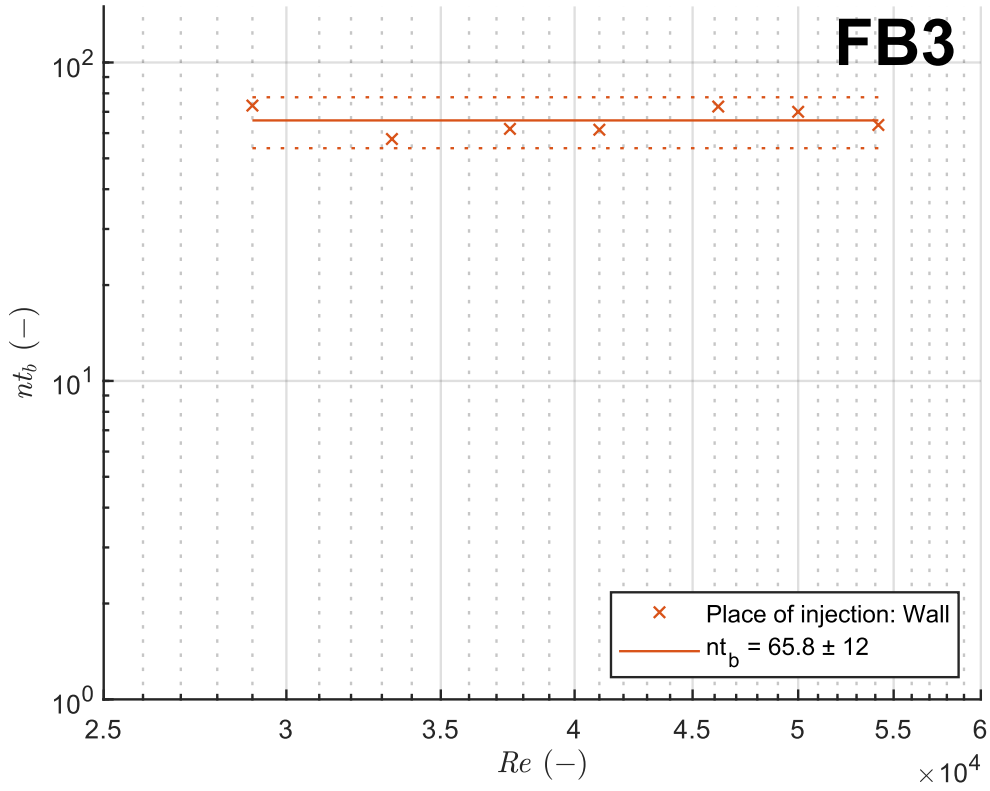
FB3
$10^2$
$10^1$
$10^0$
$nt_b$ $(-)$
2.5
3
3.5
4
4.5
5
5.5
6
$Re$ $(-)$
$\times 10^4$
Place of injection: Wall
nt$_b$ = 65.8 ± 12

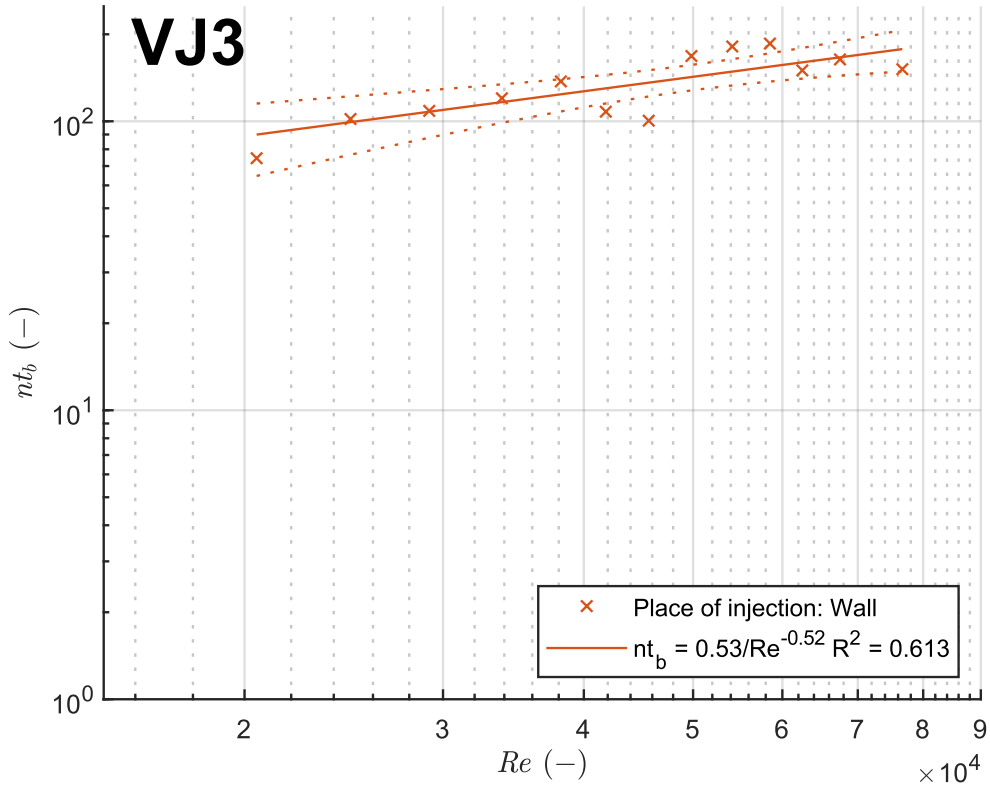
VJ3
$10^2$
$10^1$
$10^0$
$nt_b$ $(-)$
2
3
4
5
6
7
8
9
$Re$ $(-)$
$\times 10^4$
Place of injection: Wall
nt$_b$ = 0.53/Re$^{-0.52}$ R$^2$ = 0.613

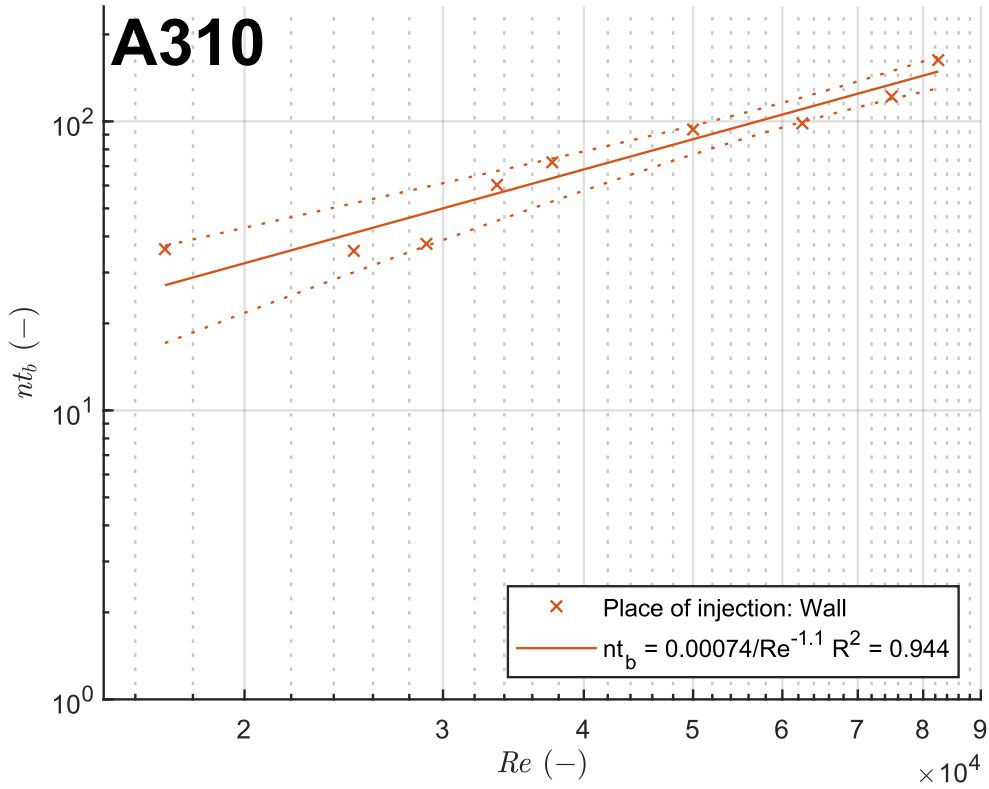


***Fig. 14.*** *Dimensionless blending time of agitators as a function of Re*

***Tab. 2.*** *Overview of* regression *parameters from agitator blending*

| *Agitator type* | *A* | *B* | $R^2$ | *Re (-)* |
|---|---|---|---|---|
| ***Cylinder*** | | | | |
| *PB6 with baffles* | 55 ± 14 | 0 | - | From 25 000 |
| *PB6 without baffles* | 85 ± 21 | 0 | - | From 25 000 |
| *PB6 literature (99 %)* | 46.3 | 0 | - | From 10 000 |
| ***Sphere*** | | | | |
| *PB6 – wall inj.* | 8 e+7 | 1.4 | 1 | 17 000 – 29 000 |
| *PB6 – wall inj.* | 27.6 ± 6.8 | 0 | - | From 29 000 |
| *PB6 – axel inj.* | 3.4 e+8 | 1.6 | 1 | 17 000 – 29 000 |
| *PB6 – axel inj.* | 23.6 ± 4.0 | 0 | - | From 29 000 |
| *RT6 – wall inj.* | 5 e+4 | 1.1 | 0.87 | 17 000 – 38 000 |
| *RT6 – axel inj.* | 55 ± 28 | 0 | - | 17 000 – 38 000 |
| *FL3* | 65.8 ± 12 | 0 | - | From 29 000 |
| *VJ3* | 0.53 | -0.52 | 0.61 | 20 000 – 77 000 |
| *A310* | 7 e-4 | -1.1 | 0.94 | 17 – 83 000 |

### 3.1.2 Results of jet blending

As discussed in chapter 1.2.3.2, jet blending may be described using several different approaches. A decision was made to test which method found in the literature is more suitable for our geometry jet position sets. Based on the analysis from the same chapter, which concluded that the underlying theory is similar to that of the agitators, similar outcomes were expected. That means that in the creeping flow region the value of dimensionless time is supposed to be constant and in the turbulent region a similar result with different value is to be expected. In-between these regions, a transition region should appear. Similarly, due to its simplicity and the ability to transition into a constant, a power function (46) was used for the regressions. To determine the influence of the B parameter, the T-test was applied to the regression. In the case where the parameter B was deemed unnecessary, the approximation using the mean value was used instead. For all regressions, the Student's confidential interval was calculated and is presented in the corresponding figures.

In Fig. 15., the data analysed using the pipe model are presented. The dimensionless time was calculated using equation (38) and the value of $Re_{tr}$ according to equation (32). In Fig. 16. the second model based on the vessel was used. The value of dimensionless time was calculated using equation (34). In this case, however, an additional parameter D/d was added to satisfy the result of the analysis displayed in equation (43), thou unnecessary, as there were no other geometries to compare the effect of this parameter to. Due to the different approaches to the problem, a different value of $Re_V$ had to be calculated using equation (37). The resulting regression parameters from this set of experiments are presented in the Tab. 3.

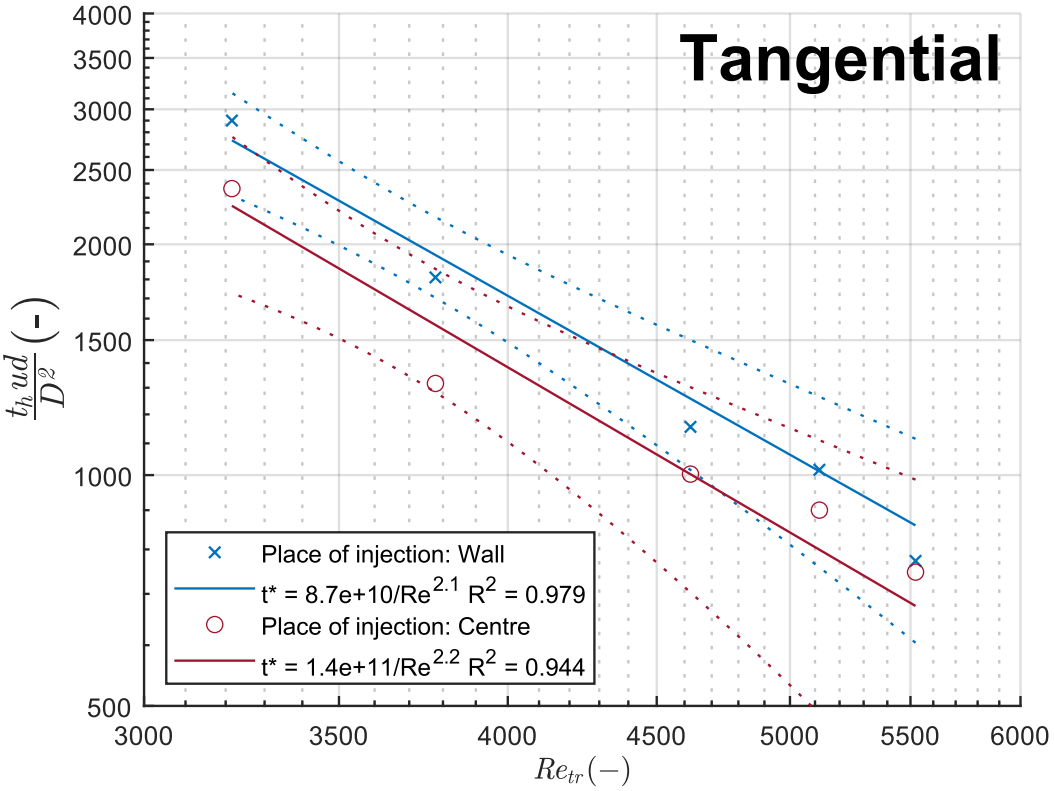
Tangential
4000
3500
3000
2500
2000
1500
1000
500
3000
3500
4000
4500
5000
5500
6000
$\frac{t_h ud}{D^2}$ (-)
$Re_{tr}(-)$
Place of injection: Wall
t* = 8.7e+10/Re^2.1 R^2 = 0.979
Place of injection: Centre
t* = 1.4e+11/Re^2.2 R^2 = 0.944

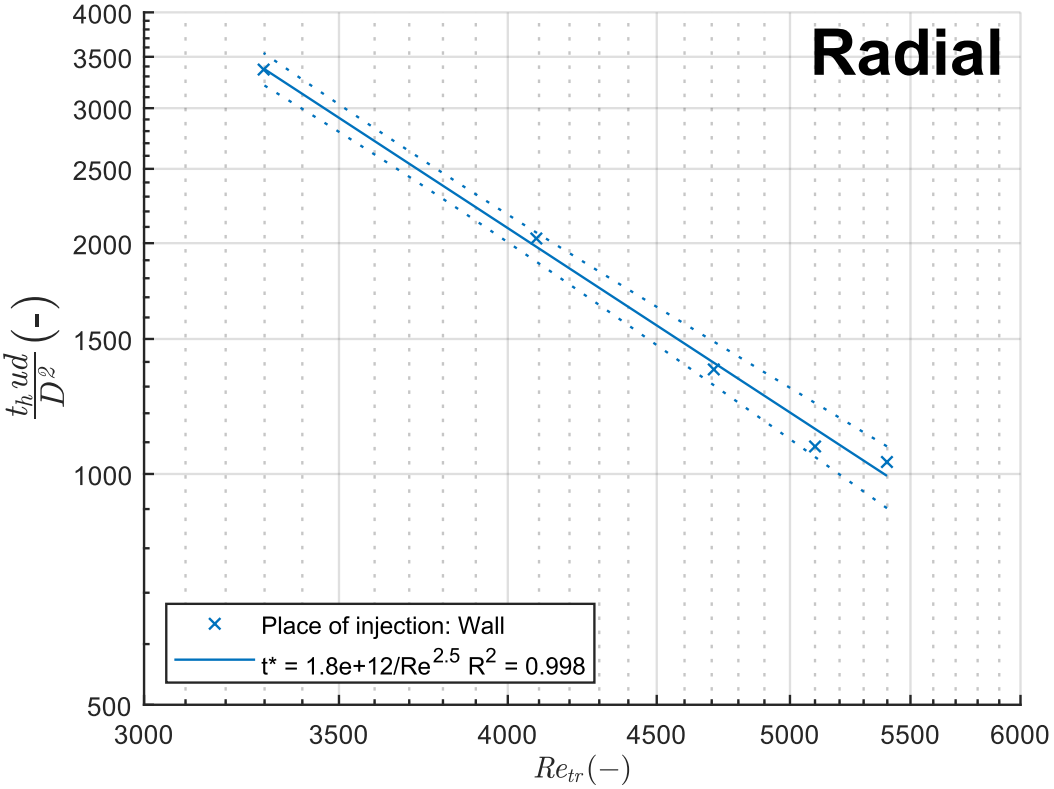
Radial
4000
3500
3000
2500
2000
1500
1000
500
3000
3500
4000
4500
5000
5500
6000
$\frac{t_h ud}{D^2}$ (-)
$Re_{tr}(-)$
Place of injection: Wall
t* = 1.8e+12/Re^2.5 R^2 = 0.998

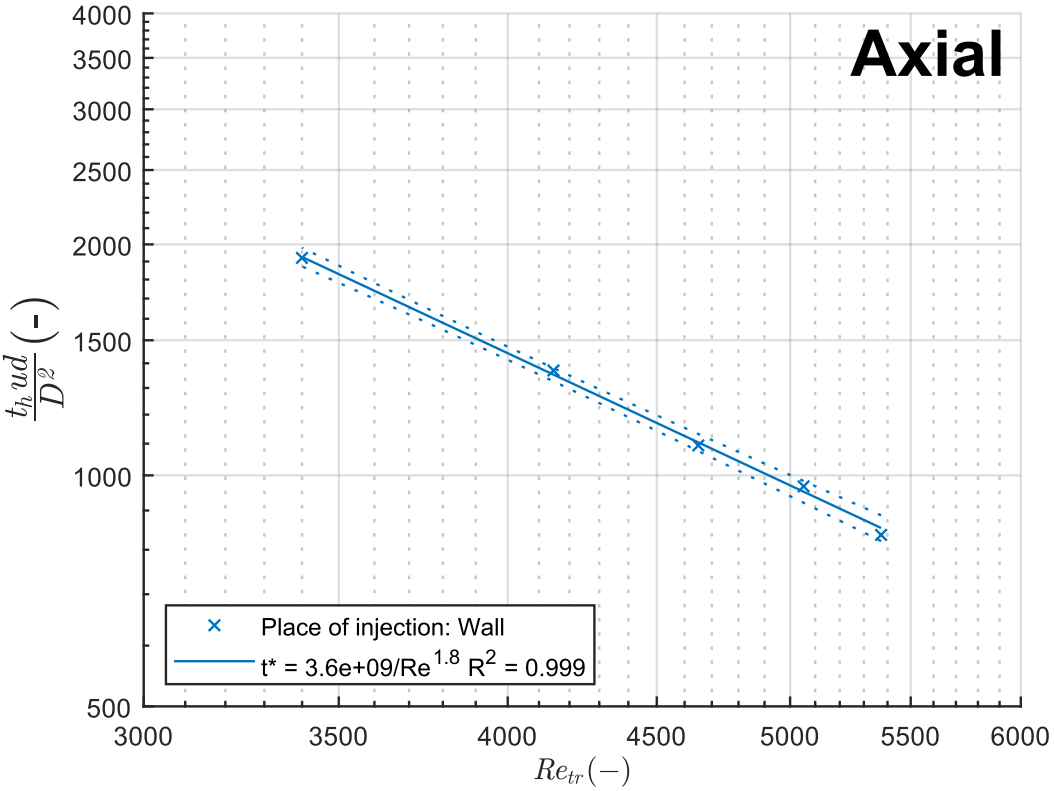


***Fig. 15.*** *t* as a function of Re for different inlet-outlet positions based on the pipe model*

*Caption: Positioning of the jet nozzle*

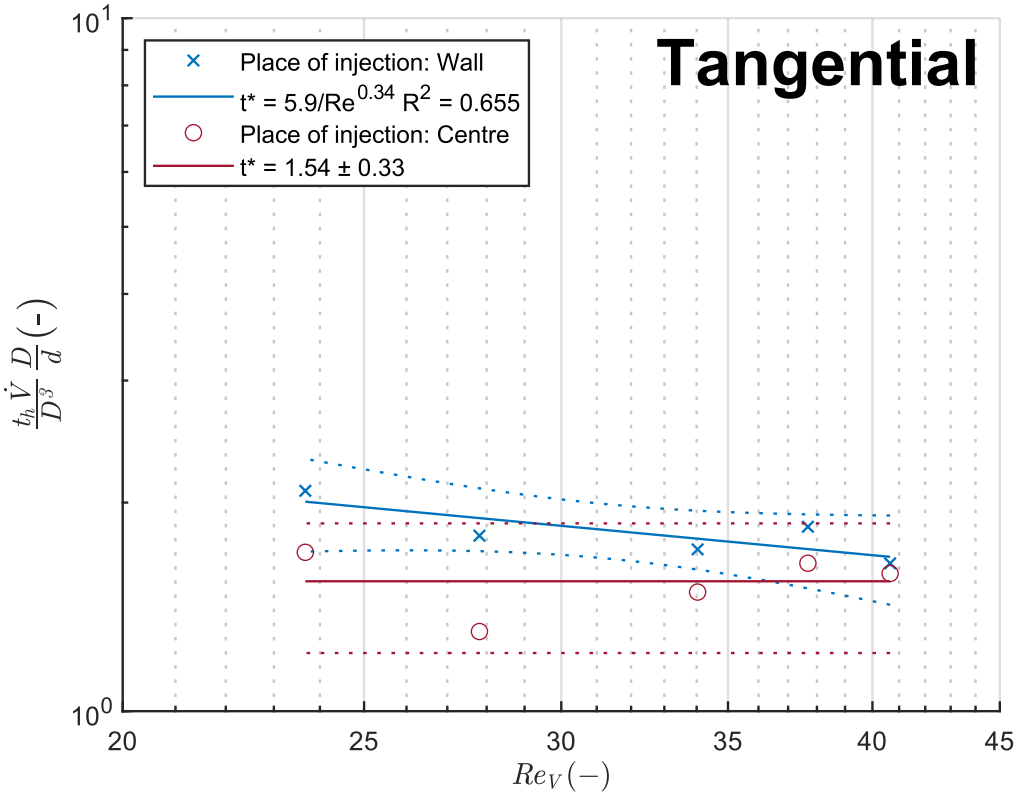

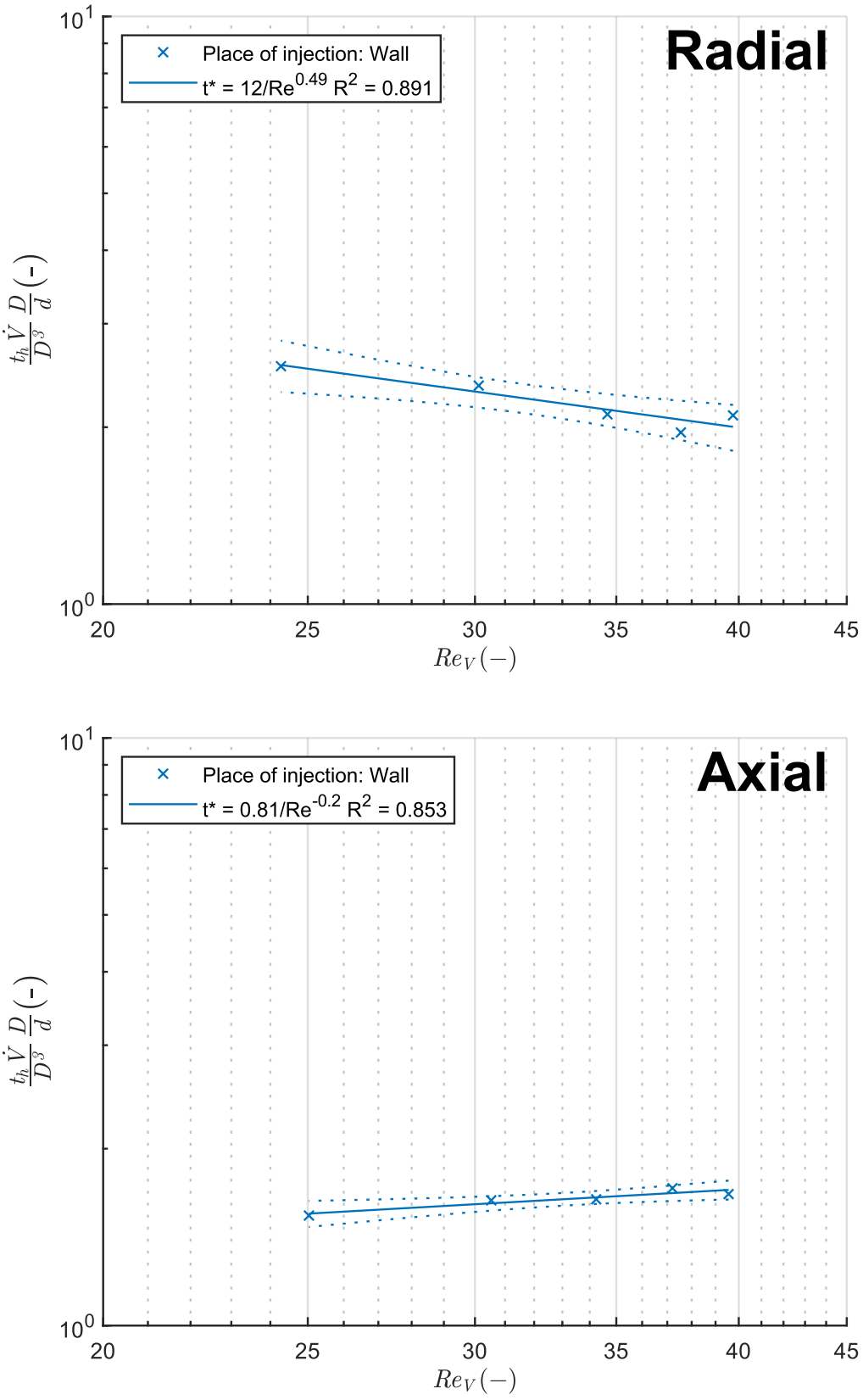


***Fig. 16.*** *t* as a function of Re for different inlet-outlet positions based on the vessel model*

*Caption: Positioning of the jet nozzle*

***Tab. 3.*** *Overview of* regression *parameters from jet blending*

| *Inlet position* | *A* | *B* | $R^2$ | *Re (-)* |
|---|---|---|---|---|
| ***Pipe model*** | | | | |
| *Tangential – wall inj.* | 9 e+10 | 2.1 | 1 | 3000 – 6000 |
| *Tangential – centre inj.* | 1 e+11 | 2.2 | 0.94 | 3000 – 6000 |
| *Radial* | 1.8 e+12 | 2.5 | 1 | 3000 – 6000 |
| *Axial* | 3.6 e+9 | 1.8 | 1 | 3000 – 6000 |
| ***Vessel model*** | | | | |
| *Tangential – wall inj.* | 6 | 0.3 | 0.66 | 20 – 45 |
| *Tangential – centre inj.* | 1.5 ± 0.3 | 0 | - | 20 – 45 |
| *Radial* | 12 | 0.5 | 0.89 | 20 – 45 |
| *Axial* | 0.8 | -0.2 | 0.85 | 20 – 45 |

As can be seen in Tab. 3., the pipe model seems to better fit the measured data with the values of $R^2$ around 1. Additionally, as the main benefit of the vessel model, its ability to scale with the size of the vessel cannot be tested and thus cannot be verified as accurate. For these reasons, only the pipe model regressions will be used in the following chapters.

Additionally, the homogenisation time when injecting next to the wall was worse than when injecting near the centre of the vessel. This result suggests that the difference, which was seen in Fig. 14. was not caused purely by the varying point of injection and the proximity to the agitator. Additionally, in this case the injection towards the wall had the benefit of the proximity of the inlet, suggesting that when the injection was directed towards the centre, the initial impulse was sufficient to transport the added liquid faster towards the outlet at the bottom of the vessel enabling swifter distribution.

To conclude, since all other measurements throughout this thesis were measured using the worst possible injection position, the wall injection data will be used for the energy assessment in the following chapters.

### 3.1.3 Results of pneumatic blending

The last set of experiments described in chapter 2.1 was blending using a sparger unit. Compared to the previous chapters, due to the lack of underlying theory found in the literature, no additional adjustments to the measured data were made. A regression using the redefined power function (48) was used again, as the nature of the problem remains the same. The regression parameters are displayed in the Tab. 4. and the measured data in Fig. 17.

$$t = \frac{A}{\dot{V}^B} \tag{48}$$

***Tab. 4.*** *Overview of* regression *parameters from pneumatic blending*

| | $A$ | $B$ | $R^2$ | $\dot{V}$ *(L/min)* |
|---|---|---|---|---|
| *Sparger* | 42 | 0.2 | 0.66 | 3.5 – 35 |

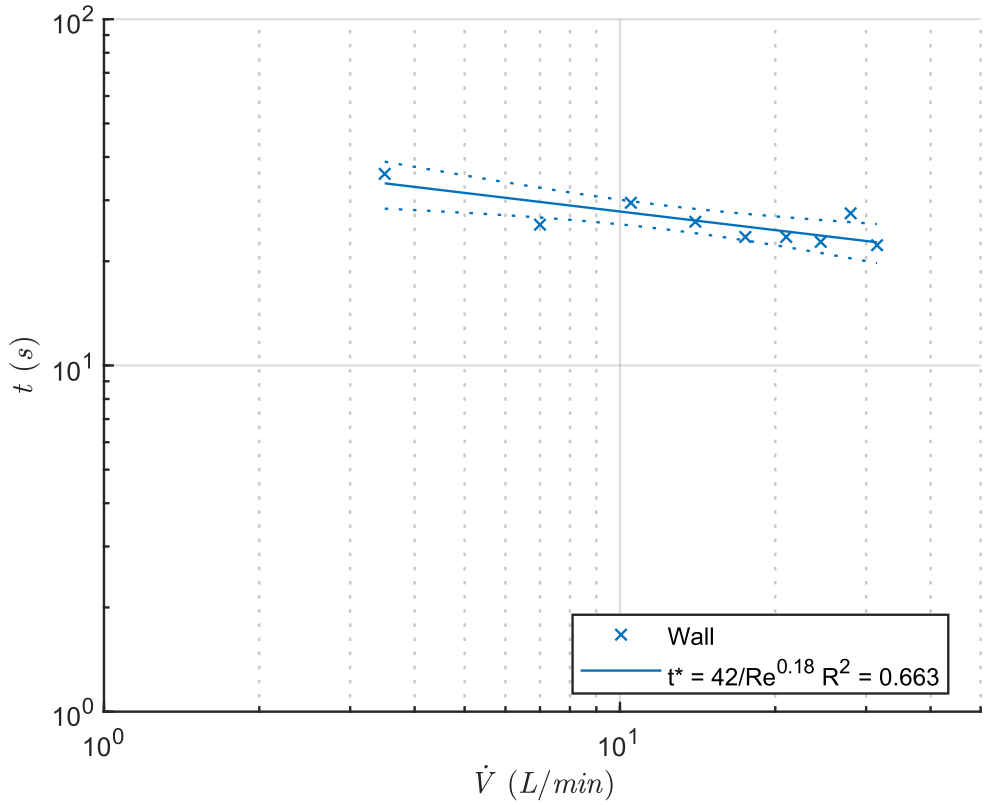


***Fig. 17.*** *t as a function of* $\dot{V}$ *for pneumatic blending*

## 3.2 Agitator power input

The assessment of power consumption of an agitator system is a well-researched topic as was discussed in chapter 2.2. The power number Po is used for this purpose and is defined using equation (24). As was introduced in chapter 1.2.2.2 two extremes may be distinguished. At low values of Re, the mixing is performed under creeping flow conditions and the product of Re·Po is constant, as shown in equation (25). At the opposite extreme, at high values of Re, the value of Po itself should be constant (eq. (26)). As these equations represent the extremes of the applied dimensionless analysis, a third intermediate equation (49) was used. It was chosen due to its simplicity and its ability to converge to either of the mentioned results. To test whether exponent B has a significant role in the regression function, the T-test was applied to the regression result. When deemed insignificant, an approximation by an average value (B = 0) was used instead. For every regression, a Student's confidence interval was calculated and is presented with the corresponding regression.

$$Po = \frac{A}{Re^B} \tag{49}$$

To transform the measured data into the desired form, several modifications had to be made. The measured torque value had to be calculated using equation (49). For this calculation the conversion constant $k_M$ was determined using the calibration measurement, which will be discussed later in this chapter.

$$M_k = U \cdot k_M \tag{50}$$

Using the torque value and the rotation speed, the power input of the agitator to the system can be calculated using equation (51). The value of Po can be subsequently calculated using its definition (eq.(24)) and is plotted as a function of Re defined by equation (13) from chapter 1.2.2.1.

$$P = \frac{M_k \cdot n}{60} \tag{51}$$

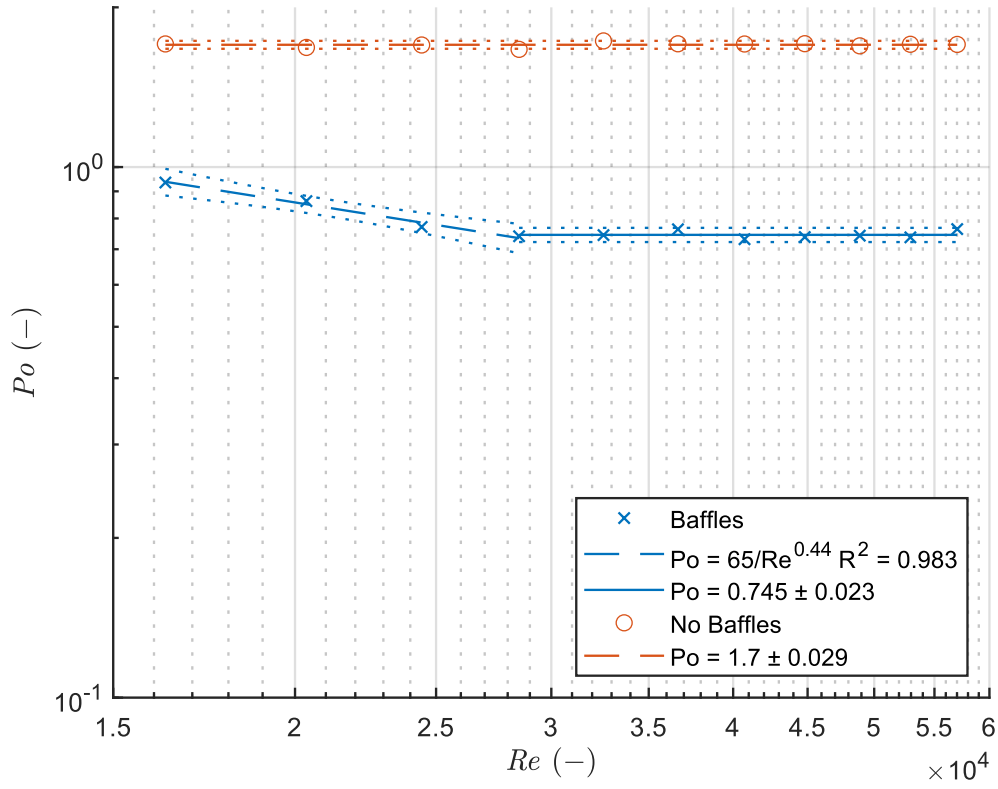


***Fig. 18.*** *Po as a function of Re in a cylindrical vessel with the PB6 agitator*

The first set of measurements was the calibration of the measuring system. Calibration was performed on the cylindrical vessel with baffles as was discussed in chapter 2.2. In the beginning, the value of $k_m$ was set to 1 and the results were assessed only graphically, the important part being the constant value of Po as found in the literature. As expected, the Po value was constant for Re greater than 15 000 but was not equal to 1.7 [27], therefore the value of $k_m$ had to be modified to fit this criterion. A MATLAB script was used for this purpose utilizing the fzero function. The resulting data is presented in Fig. 18. Additional measurement on the same vessel but without baffles was also made. It is apparent that for this setup the turbulent flow develops at higher Re values, hence both transient and turbulent regions are apparent in the data. Due to this reason, both regression using the power function and approximation using a mean value were used, with the changeover at around the Re of 28 500.

After the calibration, the experiments were performed on the spherical vessel. As was discussed in chapter 2.2 several different agitators were tested, with the accumulated results presented in Fig. 19. The complete overview of the regression parameters used to fit the presented data is shown in Tab. 5. Only transition or developed turbulent regions should appear in the data, as the Re values were too high.

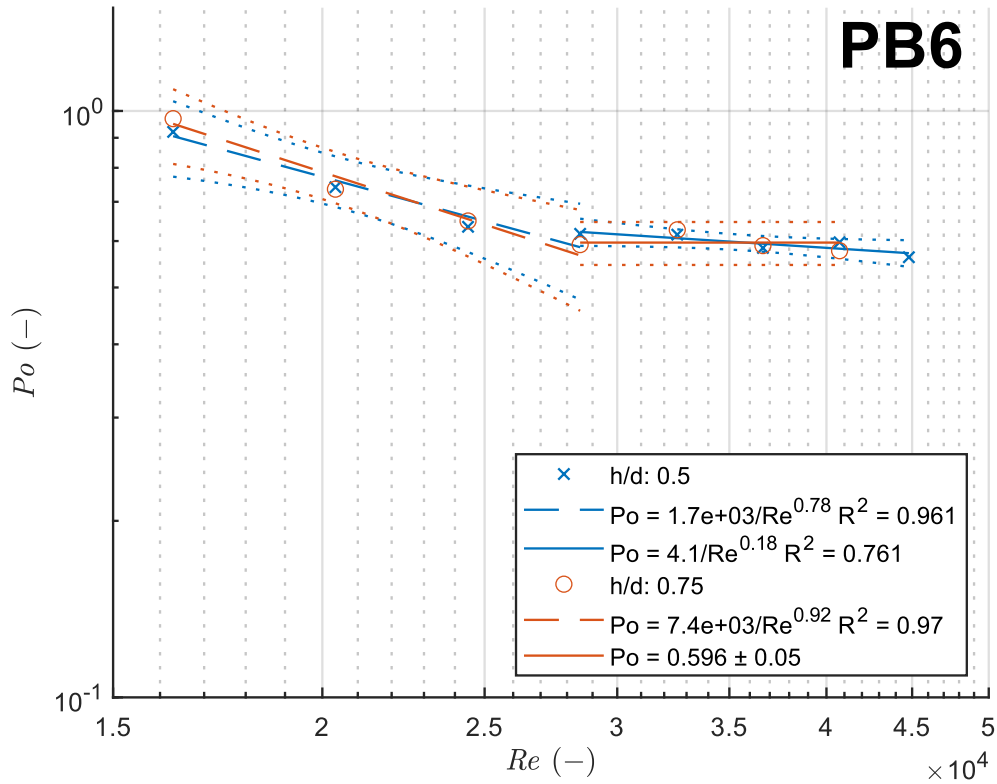
PB6
$10^0$
$10^{-1}$
$Po\ (-)$
1.5
2
2.5
3
3.5
4
4.5
5
$Re\ (-)$
$\times 10^4$
h/d: 0.5
Po = 1.7e+03/Re$^{0.78}$ R$^2$ = 0.961
Po = 4.1/Re$^{0.18}$ R$^2$ = 0.761
h/d: 0.75
Po = 7.4e+03/Re$^{0.92}$ R$^2$ = 0.97
Po = 0.596 ± 0.05

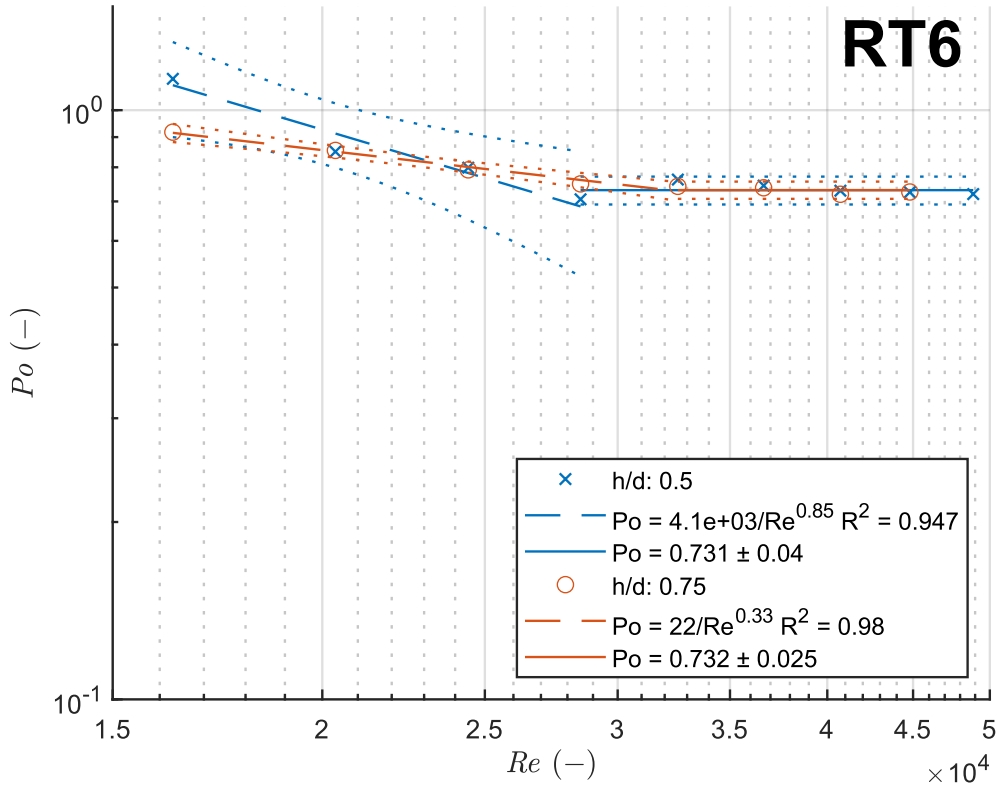
RT6
$10^0$
$10^{-1}$
$Po\ (-)$
1.5
2
2.5
3
3.5
4
4.5
5
$Re\ (-)$
$\times 10^4$
h/d: 0.5
Po = 4.1e+03/Re$^{0.85}$ R$^2$ = 0.947
Po = 0.731 ± 0.04
h/d: 0.75
Po = 22/Re$^{0.33}$ R$^2$ = 0.98
Po = 0.732 ± 0.025

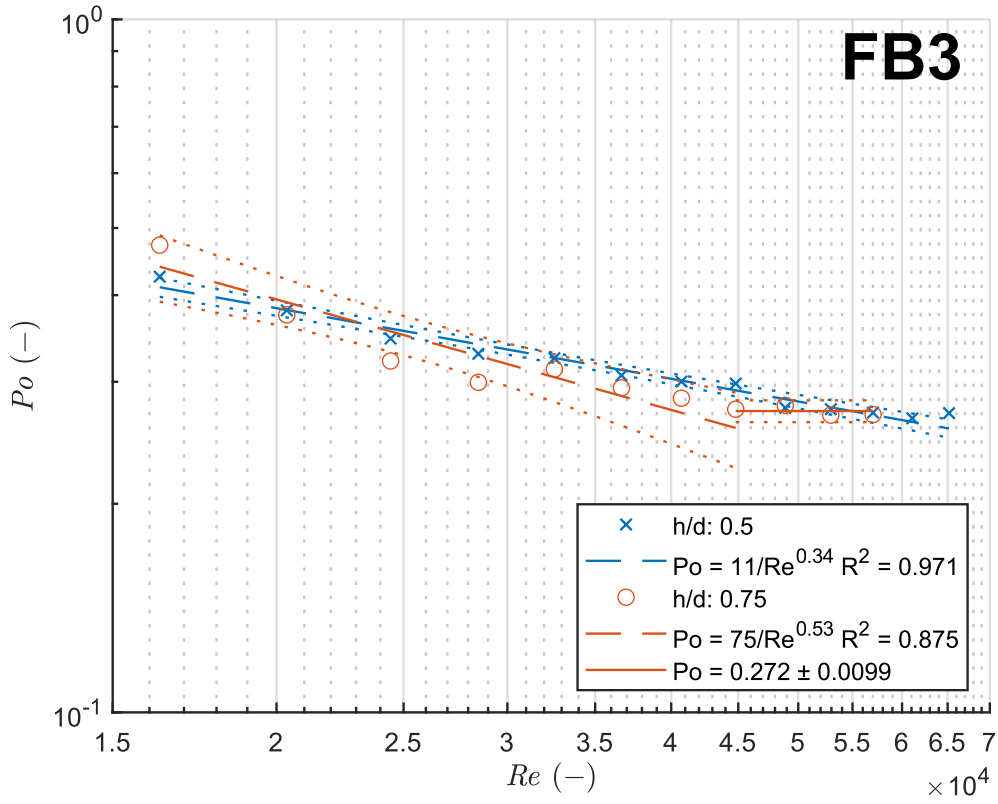
FB3
$10^0$
$10^{-1}$
$Po\ (-)$
1.5
2
2.5
3
3.5
4
4.5
5
5.5
6
6.5
7
$Re\ (-)$
$\times 10^4$
h/d: 0.5
Po = 11/Re$^{0.34}$ R$^2$ = 0.971
h/d: 0.75
Po = 75/Re$^{0.53}$ R$^2$ = 0.875
Po = 0.272 ± 0.0099

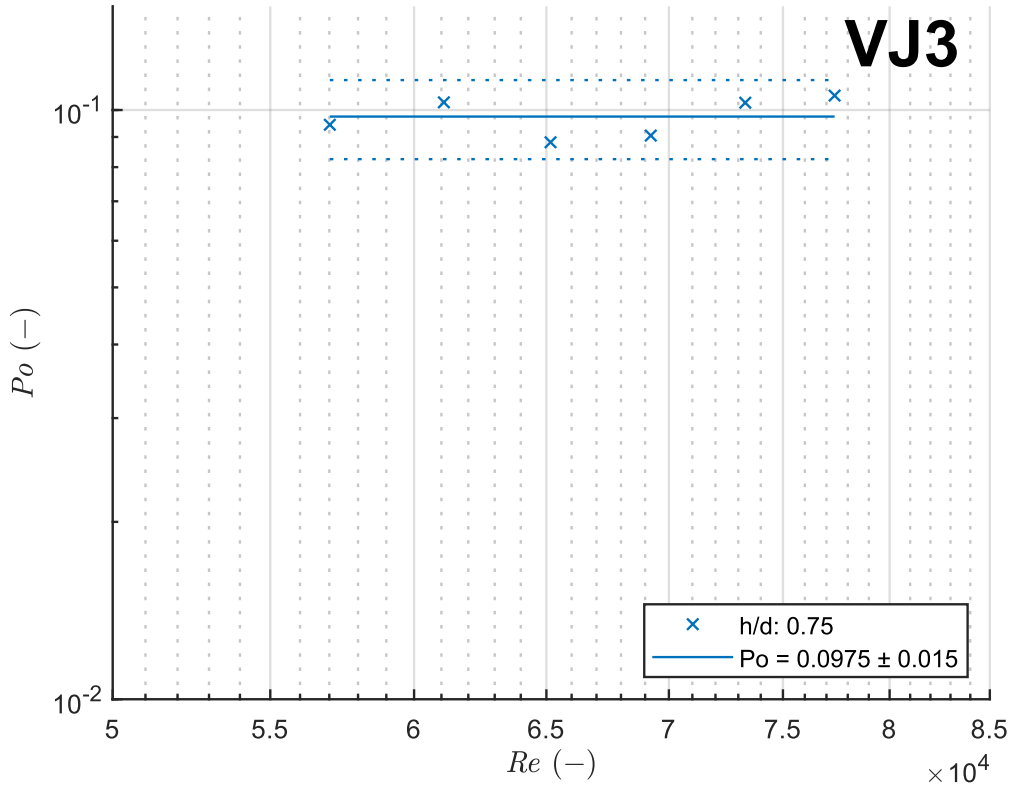
VJ3
$10^{-1}$
$10^{-2}$
$Po\ (-)$
5
5.5
6
6.5
7
7.5
8
8.5
$Re\ (-)$
$\times 10^4$
h/d: 0.75
Po = 0.0975 ± 0.015

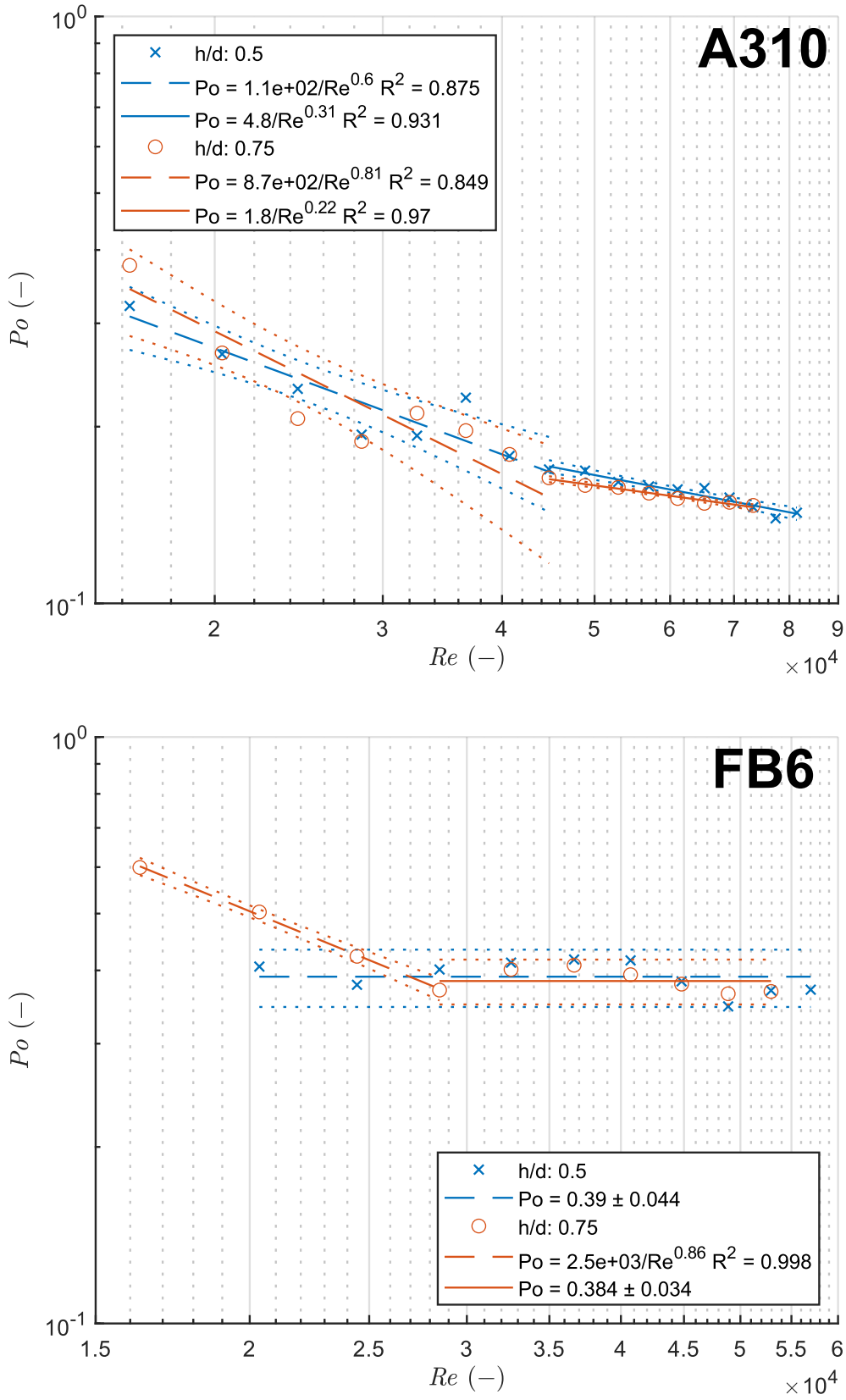


***Fig. 19.*** *Po as a function of Re for different types of agitators*

***Tab. 5.*** *Overview of the regression parameters from Po measurements*

| *Agitator* | *A* | *B* | $R^2$ | *Re (-)* |
|---|---|---|---|---|
| ***Cylinder, h/d = 1*** | | | | |
| *PB6 w. baffles* | 1.7 ± 0.03 | 0 | - | From 16 000 |
| *PB6 wo. baffles* | 65 | 0.4 | 0.98 | 16 000 – 29 000 |
| *PB6 wo. baffles* | 0.75 ± 0.02 | 0 | - | From 29 000 |
| ***Sphere, h/d = 0.5*** | | | | |
| *PB6* | 1.7 e+3 | 0.8 | 0.96 | 17 000 – 29 000 |
| *PB6* | 4.1 | 0.2 | 0.76 | 29 000 – 45 000 |
| *RT6* | 4 e+3 | 0.9 | 0.95 | 17 000 – 29 000 |
| *RT6* | 0.73 ± 0.04 | 0 | - | From 29 000 |
| *FB3* | 11 | 0.34 | 0.97 | 17 000 – 65 000 |
| *VJ3* | 0.10 ± 0.02 | 0 | - | From 56 000 |
| *A310* | 110 | 0.6 | 0.88 | 17 000 – 45 000 |
| *A310* | 4.8 | 0.31 | 0.93 | 12 000 – 82 000 |
| *FB6* | 0.39 ± 0.04 | 0 | - | From 20 000 |
| ***Sphere, h/d = 0.75*** | | | | |
| *PB6* | 7 e+3 | 0.9 | 0.97 | 17 000 – 29 000 |
| *PB6* | 0.60 ± 0.05 | 0 | - | From 25 000 |
| *RT6* | 22 | 0.3 | 0.98 | 17 000 – 32 000 |
| *RT6* | 0.73 ± 0.03 | 0 | - | From 45 000 |
| *FB3* | 75 | 0.5 | 0.88 | 17 000 – 45 000 |
| *FB3* | 0.27 ± 0.01 | 0 | - | From 45 000 |
| *A310* | 870 | 0.81 | 0.85 | 17 000 – 45 000 |
| *A310* | 1.8 | 0.22 | 0.97 | 45 000 – 74 000 |
| *FB6* | 2.5 e+3 | 0.86 | 0.99 | 17 000 – 28 000 |
| *FB6* | 0.39 ± 0.03 | 0 | - | From 28 000 |

Based on the data presented above, it may be concluded that the majority of the agitators operated in the transition region. The only agitator that reliably entered the region of developed turbulent flow was RT6. The results for PB6 were perhaps skewed by error as based on the homogenisation measurement, a behaviour similar to that of RT6 was expected. The interval of measurement was shortened for VJ3 as at lower values of Re the agitator did not work properly.

## 3.3 Results of particle suspension

The last of the experiments carried out in this thesis was the assessment of the agitator's ability to suspend particles. Only a selection of agitator types was used for these experiments, as discussed in chapter 2.3. The gathered data is presented in Tab. 6. However, full suspension was never achieved during the experiments; as at high rotation speeds, a large central vortex was forming, limiting a further increase in rotation speed. Additionally, the shape of the vessel was undermining the lifting effect, as the agitators rarely achieved lifting particles significantly higher than above the middle of the sphere. This may be caused by the curvature of the vessel and by the dominant tangential flow, as the rising particles do not have enough energy in this direction and are being redirected from the upward trajectory back down or towards the middle of the vessel. Therefore, to illustrate how effective the agitators were to lift the particles from the bottom, the height of the cloud of suspended particles was also measured.

The method used for this assessment was to compare the power density necessary to achieve the suspension of all added glass beads. The power density was calculated using equation (52). In this equation, the total volume of fluid with added particles was used. The power input was calculated from Po using equation (53). The value of Po was calculated using the regressions from chapter 3.2.

$$\varepsilon = \frac{P}{V} \tag{52}$$

$$P = Po \cdot \rho n^3 d^5 \tag{53}$$

***Tab. 6.*** *The results of particle suspension*

| *Agitator* | $c_V$ *(% vol.)* | $n_s$ *(1/min)* | $\varepsilon$ *(W/m$^3$)* | $h_p$ *(mm)* |
|---|---|---|---|---|
| *PB6* | 2.44 | 264 | 37 | 110 |
| *A310* | 2.44 | 468 | 50 | 110 |
| *RT6* | 2.44 | 207 | 23 | 115 |
| *FB3* | 2.44 | 354 | 42 | 110 |
| *FB6* | 2.44 | 300 | 32 | 120 |
| *PB6* | 4.77 | 270 | 38 | 110 |
| *RT6* | 4.77 | 219 | 27 | 80 |
| *FB6* | 4.77 | 309 | 36 | 90 |
| *RT6* | 6.98 | 219 | 26 | 100 |
| *RT6* | 9.1 | 231 | 26 | 100 |
| *RT6* | 13 | 231 | 28 | 60 ~180 (wave) |

# 4 Results comparison

In this section, the results gained from the previous chapter are compared. The focus of this comparison is to choose the most suitable type of mixing device suitable for the spherical vessel. Secondly, a comparison with the data already available in the literature for various mixing devices will be presented to see whether it could be, in a modified form, used instead.

## 4.1 Evaluation of flow induced by the agitators

It is apparent from the results in chapters 3.1.1 and 3.2, that some agitators do not behave according to the theory established at the beginning of this thesis.

The most consistent results were achieved by radially pumping agitators. For PB6, the transition to the developed turbulent region for both the Po and nt seemed to occur around the Re value of 29 000. Comparing this result with the cylindrical vessel without baffles, the transition to the developed turbulent region seemed to occur slightly earlier at around Re value of 27 000, suggesting that with a more precise measurement the result found by Ameur [22] may be confirmed for this agitator. For the other radial agitator, the RT6, the homogenisation data seemed too imprecise to make any similar conclusions, but the behaviour at least looked similar in nature.

However, during the experiments, large differences in behaviour were found between the hydrofoil impellers. For the homogenisation experiments, the FB3 seemed to operate in the developed turbulent region, while the behaviour of the A310 was completely unexpected, as it kept rising with the increase in Re value. The results look even more strange when compared to the ones gained from Po measurements. Here the FB3 seemed to operate completely in the transition region while the results of A310 suggested some change to the flow behaviour around Re value of 44 000. The change, however did not comply with the established theory.

To conclude, for radial agitators, the data available in the literature might be successfully modified, since the behaviour appeared to be similar to the one found in cylindrical vessels. However, a more precise measurement will be necessary to fully confirm this result. For the axial agitators, it is apparent that the behaviour was too different even between the individual agitators. Hence, no similarly broad conclusion can be made.

## 4.2 Energy assessment of the blending process

One of the most important parameters regarding the design of industrial equipment is its power consumption, as it directly influences the operating expenses. To efficiently evaluate the energy performance of the different methods, only the best performing devices from each of the groups are presented in Fig. 23. The process of selecting the best performing representative is presented in subsequent chapters.

### 4.2.1 Agitator energy consumption

The method published in [10] was used to assess the necessary blending energy. For this purpose, the parameter defined by equation (54) was calculated. This parameter was chosen because, in the region of developed turbulent flow, its value should be constant, making the comparison easier. In this equation, Po and dimensionless time were calculated using regressions from the previous chapters. The results were subsequently plotted against the parameter presented in equation (55) and are presented in Fig. 20.

$$\frac{Pt^3}{\rho D^5} = Po \cdot (nt_b)^3 \left(\frac{d}{D}\right)^5 \tag{54}$$

$$\frac{D^2\rho}{\mu t} = \frac{Re}{nt_h}\left(\frac{D}{d}\right)^2 \tag{55}$$

From this figure, it is apparent that the two best-performing agitators are the PB6 and the RT6. In the region of the developed turbulent flow, it even surpassed the cylindrical vessel with baffles and the PB6 agitator. As both agitators pump at least partially in the radial direction, it is supposed that the direction of the induced flow is the main reason for their good results. An expanded discussion on this topic is presented in chapter 4.5.

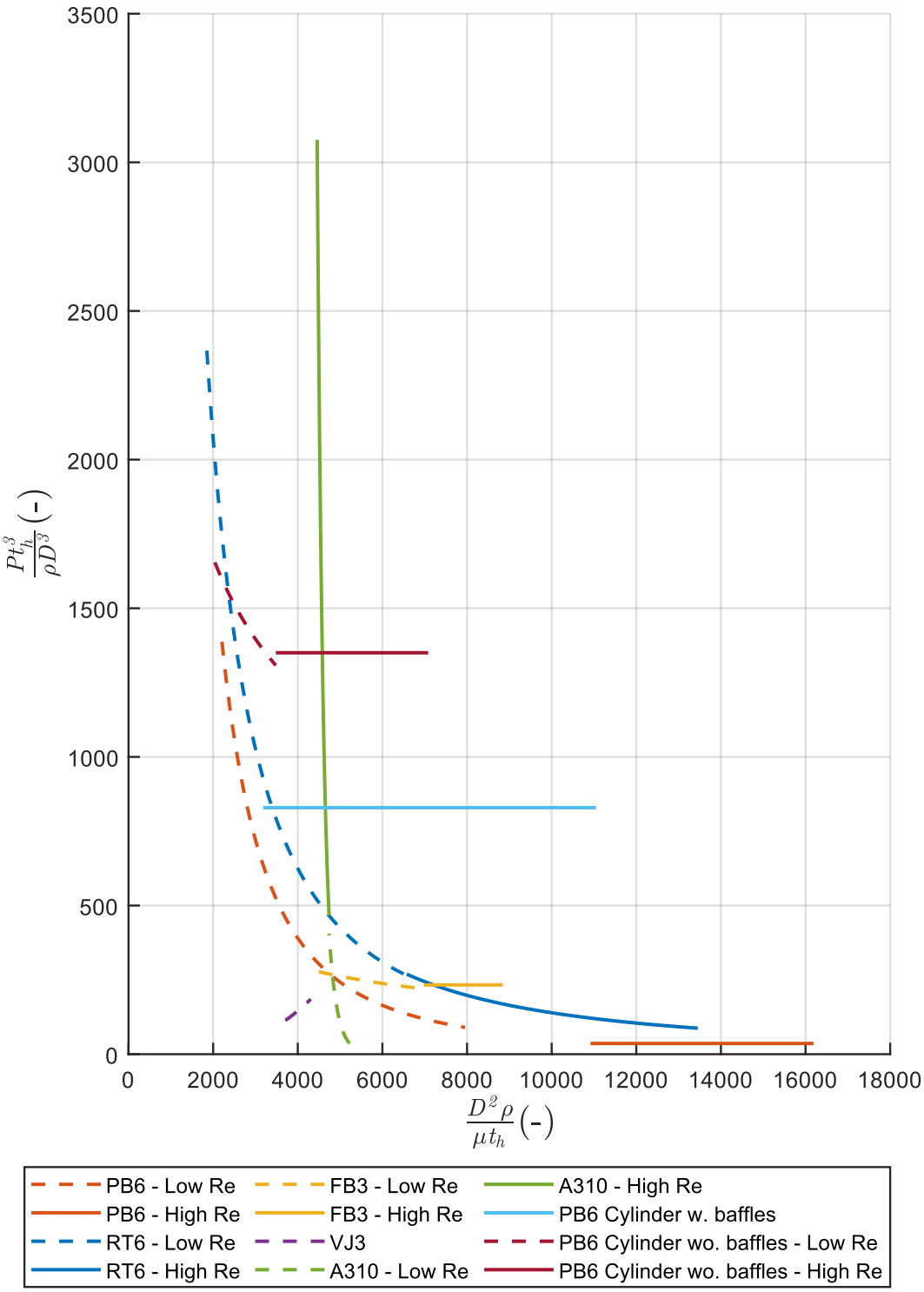


***Fig. 20.*** *Dimensionless blending energy of different jet agitator types*

### 4.2.2 Jet energy consumption

The total amount of energy necessary to circulate the liquid is introduced into the system by the pump and could therefore be easily measured at the power outlet. However, this energy is wasted mostly to overcome the drag in the tube outside of the mixing vessel. For this reason, the energy introduced into the mixed batch was assumed to be equal to the kinetic energy of the stream at the jet nozzle (eq. (56)).

$$e_k = \frac{\bar{u}^2}{2} \tag{56}$$

Consequently, the total amount of blending energy is calculated using equation (57). For this calculation, the blending time $t_b$ was calculated using the regressions gained in chapter 3.1.2. Only the pipe model was used for this purpose, as its regressions appeared to better fit the measured data. The results are then plotted against u in Fig. 21.

$$E = t_b \rho \dot{V} e_k = t_b \rho \frac{\pi d_p^2}{8} \bar{u}^3 \tag{57}$$

As the best performing configuration, the axial outlet position was chosen for comparison because of its lowest energy demand across the whole interval of nozzle speeds.

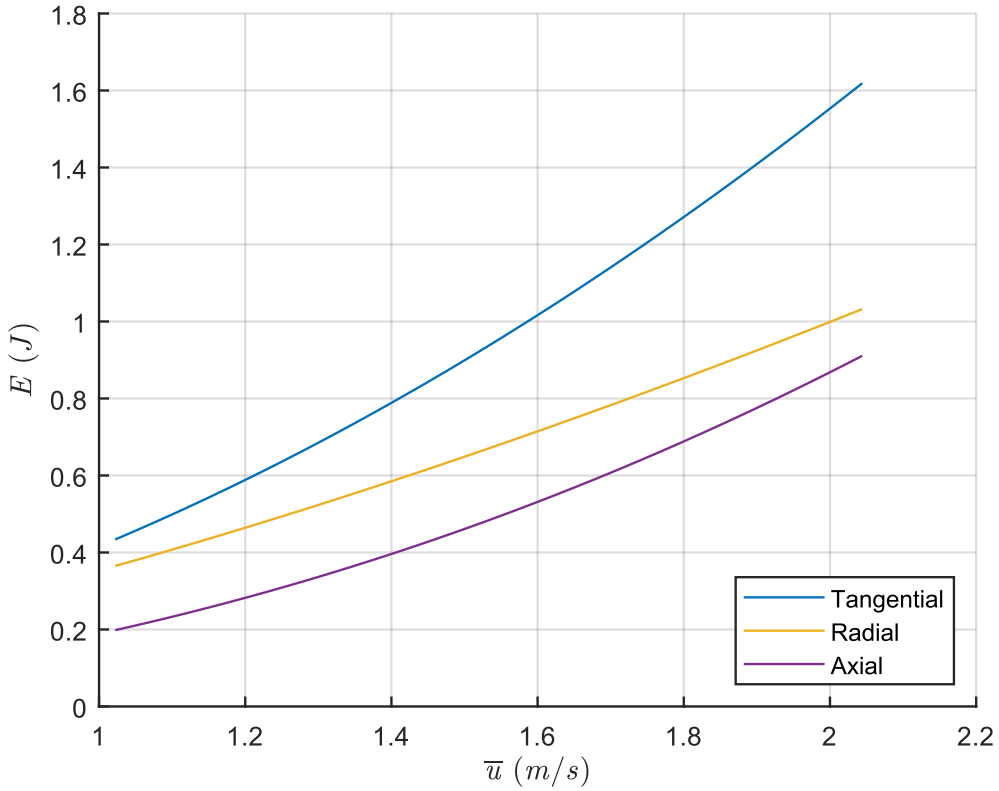


***Fig. 21.*** *Blending energy of different jet configurations*

### 4.2.3 Sparger energy consumption

A similar approach to that in the previous chapter was used to assess the energy requirements of the sparger unit. During the experiment described in chapter 2.1.3, the pressure loss on the unit was measured. From this measurement, the energy loss can be calculated using equation (58). This equation assumes negligible losses due to friction or due to minor losses between the point of measurement of the static pressure and the sparger unit. This may be assumed based on the fact that the pipe was of a short length with a very smooth surface.

$$e_z = \frac{\Delta p}{\rho} \tag{58}$$

To calculate the blending energy, equation (57) was used, where instead of the $e_k$ the $e_z$ was used. The results from this measurement are presented in Fig. 22. However, contrary to the previous chapter, only part of this energy is released into the mixed fluid as the bubbles travel too quickly to transfer all their energy before reaching the surface. Hence the required energy to mix the fluid is significantly higher than the energy used by the other assessed methods.

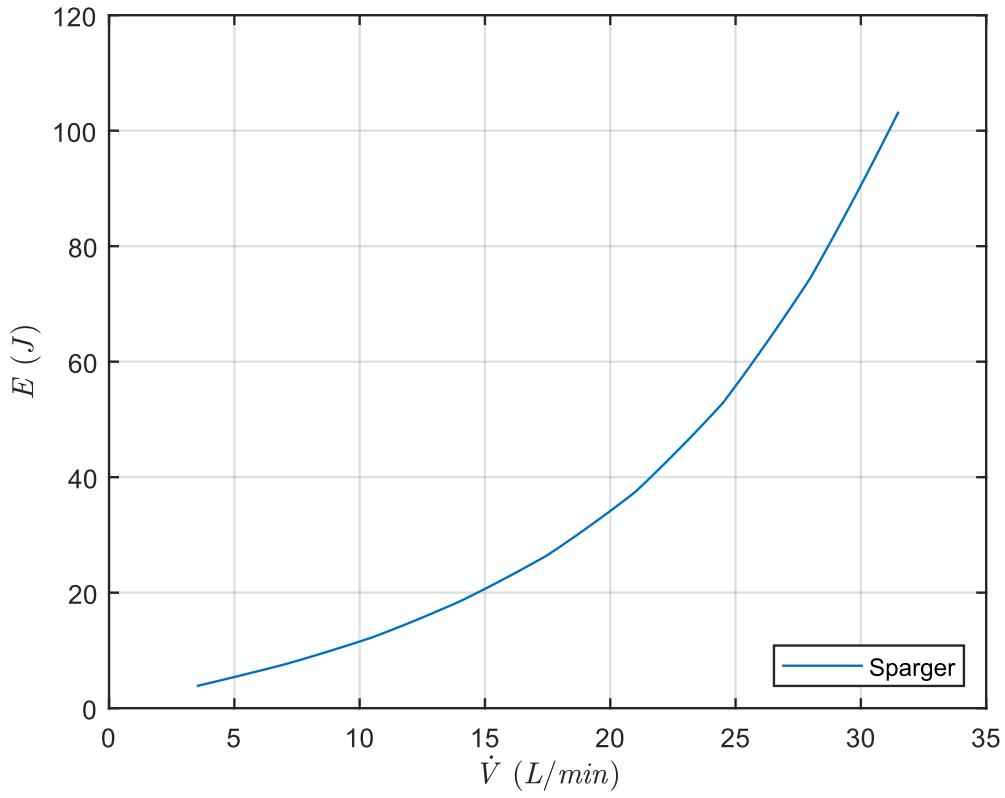


***Fig. 22.*** *Blending energy of the sparger unit*

### 4.2.4 Final energy comparison

The best-performing device was chosen from each group of mixing devices for this comparison. Of the different agitator types, the RT6 was chosen as the best overall performing agitator accompanied by PB6, due to its lowest energy demand. As the best performing jet, the axial position of the nozzle was chosen. To compare the methods, the power density (eq. (52)) was chosen for the comparison as it enables rapid design calculations of other connected devices. On the y-axis, the blending time was used to represent the swiftness of the used methods. The results are presented in Fig. 23.

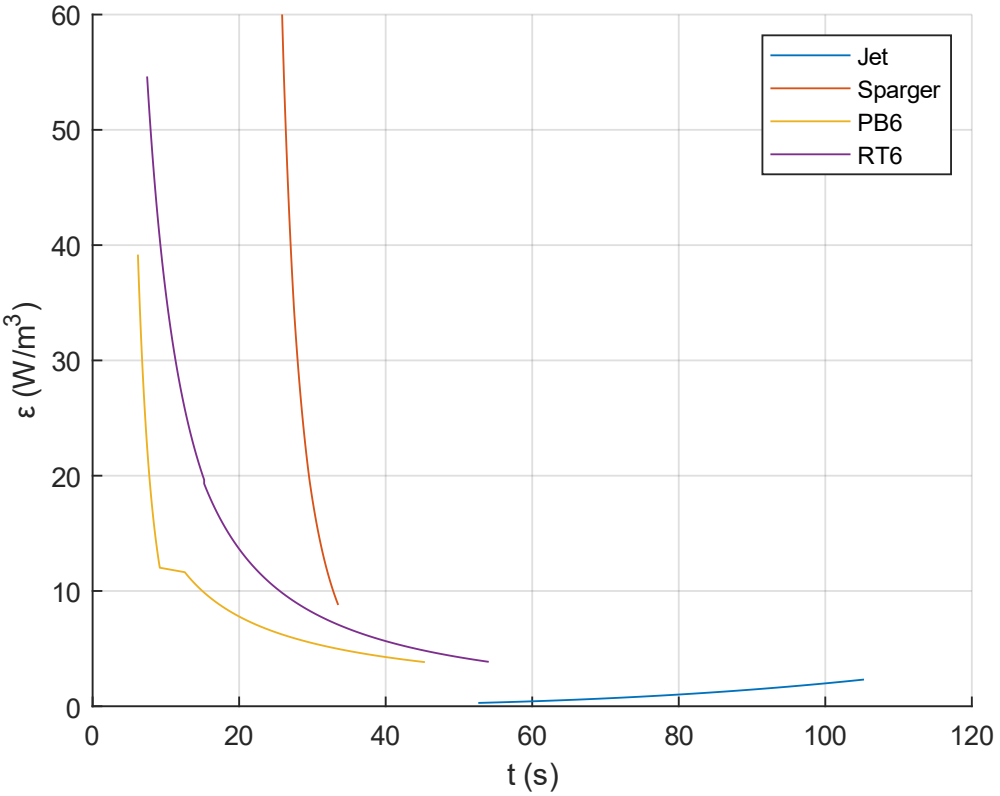


***Fig. 23.*** *Comparison of the power density necessary to achieve homogeneity*

It is apparent that, for applications where blending time is not a factor, jet-induced mixing is the optimal method of choice. An example of such an application would be mixing in fluid storage silos, an application on which the method was originally tested.

For all other general-purpose applications where a short blending time is required, an agitator unit should be used. From these, agitators with radial pumping direction seem to be the best performing.

Lastly, aerating the vessel seems like the worst option with the highest energy consumption. This, compounded by the fact that compressed air energy tends to be 7 – 8 times more expensive than an equivalent amount of electrical energy [37], makes mixing with a sparger unit only viable when the compressed gas has another use in the technology. An example of such a technology would be aerated bioreactors used in fermentation tanks or in water treatment plants.

## 4.3 Position of injection

The experimental results seem to indicate that injecting next to the wall is the worst of the locations, as the resulting blending times are all across the geometries slightly longer. Two arguments for this behaviour come to mind. In the case of agitators, when injecting towards the centre of the vessel, part of the fluid is almost immediately injected into the agitator area, distributing the fluid more rapidly throughout the vessel. But generally, the area around the axis of the vessel was the last place to get homogenized due to the low turbulence in this region. Injecting into it may disrupt the region and thus accelerate the blending.

Therefore, for the best results, the injection should be made either into the agitator area, into the highly turbulent jet stream, or into the middle of the aerated region.

## 4.4 Particle suspension

Based on the data presented in chapter 3.3, two figures are presented to illustrate the suspending effect of different agitators.

To assess the power required to achieve particle suspension, Fig. 24. was created. In this figure, the required energy density is plotted against the volume concentration of the particles inside the batch. To illustrate how effective the agitators were to lift the particles from the bottom, Fig. 25. was created to compare the height of the cloud of suspended particles with the total height of fluid in the vessel, which was about 21 cm.

From these figures, the RT6 seems like the most optimal agitator type, as it is suited for operation at the widest range of particle concentrations. However, at low particle concentrations, other agitators were also capable of suspending particles with a similar result. Moreover, all agitators had problems with achieving homogeneity. As was discussed in chapter 3.3 the probable cause is the dominant tangential flow and the geometry of the vessel. When Tacă and Păunescu added baffles [24], full homogeneity was achieved with better results than by a similar baffle-equipped cylinder.

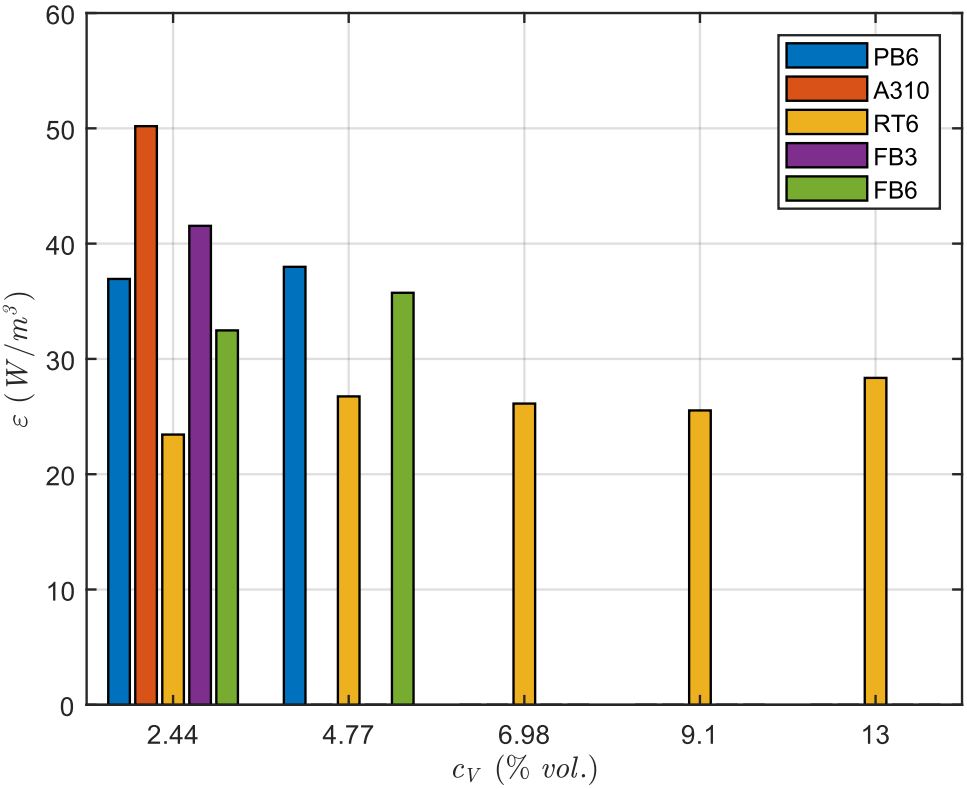


***Fig. 24.*** *The power density necessary for the suspension of particles*

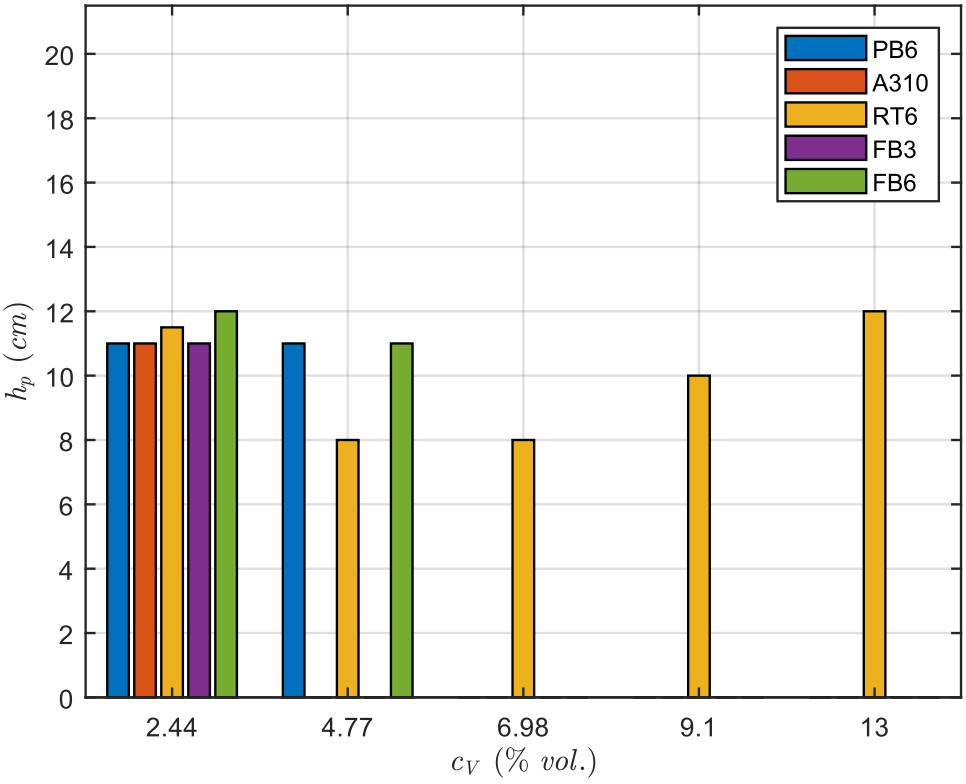


***Fig. 25.*** *Height of the cloud of suspended particles*

## 4.5 The preferred style of mixing

Based on the results reached in the previous chapters, a conclusion can be drawn that the preferred style of mixing is the one that least enhances the tangential flow. Such flows were achieved by the axial-style jet and by the sparger with the fountain-like flow pattern. The RT6 and to a lesser extent by PB6 also performed well with the radial type of pumping. These types of flow disrupt the creeping nature of the tangential flow, which is well illustrated by the difference between the Fig. 6. and Fig. 10. In the first figure, the effect of the tangential flow is apparent with the slow homogenous change in colour throughout the whole batch as the fluid slowly penetrates from the outside layers towards the centre. Contrary to that, in the second figure, it is apparent that the homogenisation is faster as the circulation circuit is far shorter, and with every circulation, part of the fluid is thrown into the yet unblended volume. To illustrate these effects, Fig. 26 is presented.

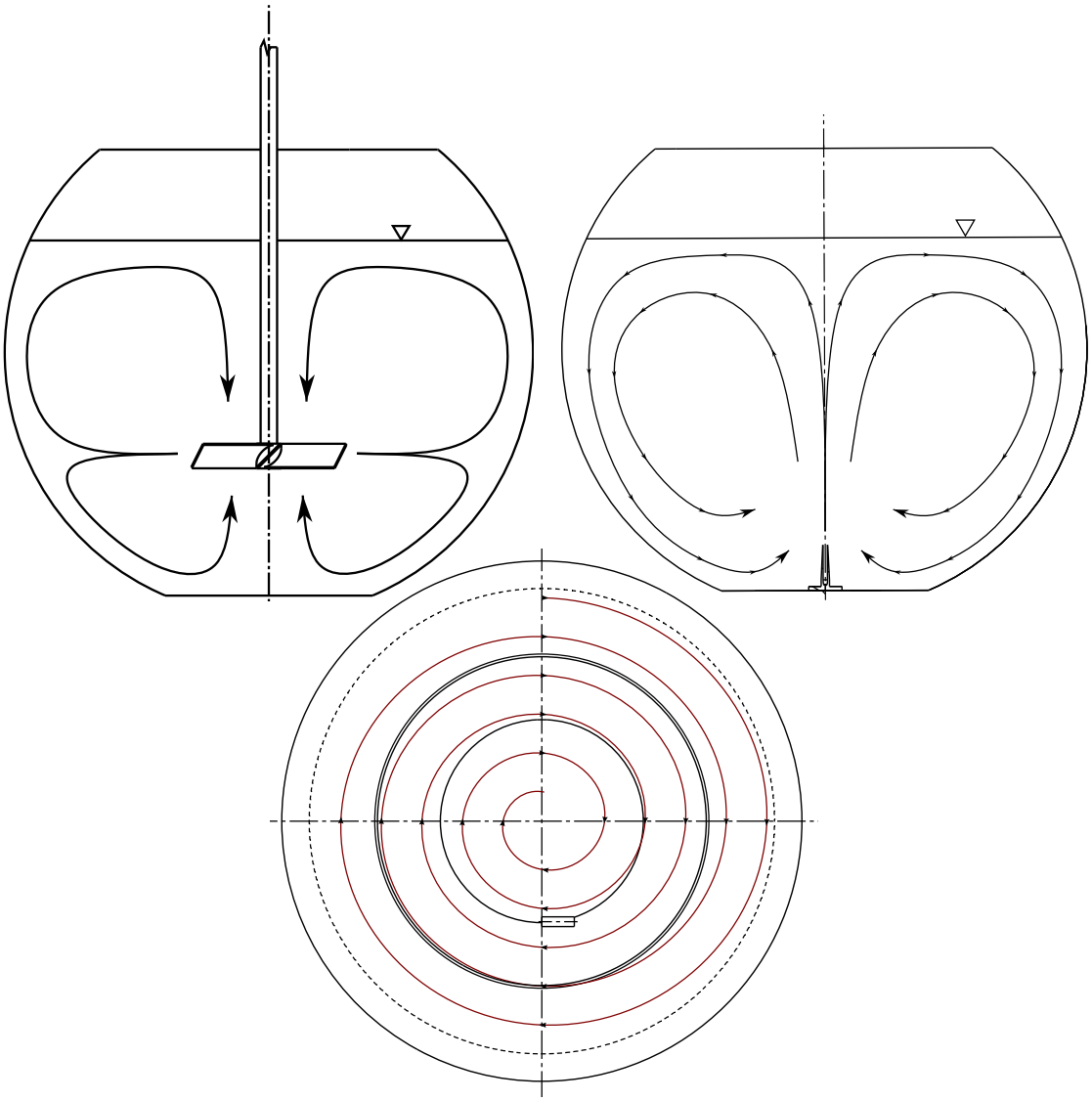

***Fig. 26.*** *Illustration of different pumping effects in the spherical vessel*

# 5 Conclusion

In this thesis, three different types of mixing devices were tested on the spherical vessel and their results were compared. The comparison was based on the power density required for the two liquids to fully blend. For the mechanical mixing, several different agitators, namely, PB6, RT6, FB3, FB6, VJ3, and A310, were chosen because of the different types of induced flow and the number of blades. The power number for each agitator was measured at various rotation speeds using a torque sensor attached to the agitator shaft. The second used method was the hydraulic mixing. Three different nozzle positions were tried, namely, radial, axial, and tangential, at various jet velocities. The energy necessary was assumed as the kinetic energy of the jet at the nozzle outlet. The third method was the pneumatic mixing, for which only one sparger type was tried. For this method, the necessary energy was set as the pressure loss on the sparger unit at different volumetric flows of compressed gas. For all mixing methods, the same Acid-Base indicator method was used to measure the homogenisation time at various flow settings.

During these experiments, the effect of tracer injection position was tested for the agitators PB6 and RT6 and the tangential jet inlet. The worse position was chosen for the method assessment. The gathered data from the experiments was interposed using a regression function according to the established theory found in literature. These regressions were used for subsequent calculations in the assessment process. Before the final assessment, the best performing option from each of the categories was chosen based on the energy required to achieve homogeneity. Finally, the best performing methods were compared based on the necessary power density to achieve homogeneity.

Additionally, for the agitators, the particle suspension capability was evaluated by the power density necessary to achieve particle suspension. Due to the agitators being incapable of achieving homogeneity of the batch at the just-suspended state, the height of the particle cloud was measured and compared.

Based on these results, the following conclusions were made:

- For applications where homogenisation time is not important, jet-induced mixing should be used due to low power consumption.
- In all applications where swift homogenisation is necessary, agitators with radial pumping seem to be the best option.
- Gas induced mixing, thou possible, should be used only if the addition of gas also serves other purpose, as the energy requirements were too high.
- The RT6 was capable of suspending particles at the widest range of concentrations. However, no agitator was able to fully homogenize the batch.
- Generally, agitators with axial flow were incapable of achieving the developed turbulent flow. The probable cause was the creation of dominating tangential flow, which hampered their performance.
- To improve performance, baffles should be added to disrupt the tangential flow.
- Without the addition of baffles, the use of characteristic agitator numbers measured on different geometries seems possible only for radial pumping agitators, as the induced flows are otherwise different in nature. However, more precise measurements will be necessary to fully verify the theory

To conclude the thesis, a final deliberation on the nature of mixing in a spherical tank is presented. It is apparent from the available data that the closest geometry is the cylindrical vessel without baffles, preferably with a dished bottom. The largest difference between these vessels is the vetted surface, which is larger for the spherical vessel. Hence, for vessels of similar diameter, the Po value measured on the spherical vessel should be higher.

Regarding the baffled cylindrical vessels and rectangular vessels, the behaviour should be different as the flow in the spherical vessel is predominantly tangential.

# 6 Sources


[1] KHAN, Fahad and Brian J. SAVILONIS. *Spherical Tanks for Use in Thermal Energy Storage Systems.* Dissertation. Worcester, USA, April 2015.

[2] SUBRAMANIAN, Bhargavi, Alexandre MIOT, Bonnie JONES, Corey KLIBERT a Krishna R. PAGILLA. A full-scale study of mixing and foaming in egg-shaped anaerobic digesters [online]. *Bioresource technology.* 2015, **192**, 461-470. Available from: DOI:10.1016/j.biortech.2015.06.023.

[3] PAUL, Edward L., Suzanne M. KRESTA and Victor A. ATIEMO-OBENG, ed. *Handbook of industrial mixing. Science and practice / edited by Edward L. Paul, Victor A. Atiemo-Obeng, Suzanne M. Kresta.* Hoboken, N.J., great Britain : Wiley-Interscience, 2004. 0-471-26919-0.

[4] TOOR, H. L. Turbulent Mixing of Two Species with and without Chemical Reactions [online]. *Industrial & Engineering Chemistry Fundamentals.* 1969, **8**(4), 655-659. Available from: DOI:10.1021/i160032a009.

[5] LINDMARK, Johan, Eva THORIN, Rebei BEL FDHILA and Erik DAHLQUIST. Effects of mixing on the result of anaerobic digestion: Review [online]. *Renewable and Sustainable Energy Reviews.* 2014, **40**, 1030-1047. Available from: DOI:10.1016/j.rser.2014.07.182.

[6] KALE, Rajesh N. and Ashwin W. PATWARDHAN. Solid Suspension in Jet Mixers [online]. *The Canadian Journal of Chemical Engineering.* 2005, **83**(5), 816-828. Available from: DOI:10.1002/cjce.5450830503.

[7] PAUL, Edward L. *Advances in Industrial Mixing. A Companion To The Handbook Of Industrial Mixing.* Hoboken New Jersey: Wiley, 2016. 0470523824.

[8] BÖHM, Lutz, Lena HOHL, Chrysoula BLIATSIOU and Matthias KRAUME. Multiphase Stirred Tank Bioreactors – New Geometrical Concepts and Scale-up Approaches [online]. *Chemie Ingenieur Technik.* 2019, **91**(12), 1724-1746. Available from: DOI:10.1002/cite.201900165.

[9] YOU, See Tiam, Abdul Aziz Abdul RAMAN, Raja Shazrin Shah Raja Ehsan SHAH and Mohamad Iskandr MOHAMAD NOR. Multiple-impeller stirred vessel studies [online]. *Reviews in Chemical Engineering.* 2014, **30**(3). Available from: DOI:10.1515/revce-2013-0028.

[10] RIEGER, František, Václav NOVÁK and Tomáš JIROUT. *Hydromechanické procesy II.* Vyd. 1. Praha : Česká technika - nakladatelství ČVUT, 2005. 8001033023.

[11] HUBBE, Martin A., Jeremy R. METTS, Daphne HERMOSILLA, M. Angeles BLANCO, Laleh YERUSHALMI, Fariborz HAGHIGHAT, Petra LINDHOLM-LEHTO, Zahra KHODAPARAST, Mohammadreza KAMALI and Allan ELLIOTT. Wastewater Treatment and Reclamation: A Review of Pulp and Paper Industry Practices and Opportunities [online]. *BioResources.* 2016, **11**(3), 7953-8091. Available from: DOI:10.15376/biores.11.3.Hubbe.

[12] ZHANG, Jun, Guangchen JIA, Minghua WANG, Shouqi CAO and Sibanda Gibson MKUMBUZI. Hydrodynamics of recirculating aquaculture tanks with different spatial utilization [online]. *Aquacultural Engineering.* 2022, **96**, 102217. Available from: DOI:10.1016/j.aquaeng.2021.102217.

[13] MACHINA, David W. and Jatinder K. BEWTRA. Bulk Mixing Using Diffused Air in Circular and Rectangular Vessels [online]. *Journal of Environmental Engineering.* 1987, **113**(1), 1-15.
Available from: DOI:10.1061/(ASCE)0733-9372(1987)113:1(1).

[14] AKHTAR, W., G. P. MATHUR and D. S. DICKEY. Mixing Design for Air Agitated Rectangular Tanks [online]. *Water Quality Research Journal.* 1980, **15**(1), 1-16. Available from: DOI:10.2166/WQRJ.1980.001.

[15] COUGHLEN, Thomas David and Theodore VERMEULEN. *POWER REAUIREMENTS FOR LIQUID AGITATION IN RECTANGULAR VESSEL* [online]. 6. June 2022 [cit. 6. June 2022].
Available from: https://escholarship.org/uc/item/4cj528w3#author.

[16] XANTHOPOULOS, CONSTANTINOS and MICHAEL STAMATOUDIS. TURBULENT RANGE IMPELLER POWER NUMBERS IN CLOSED CYLINDRICAL AND SQUARE VESSELS [online].
*Chemical Engineering Communications.* 1986, **46**(1-3), 123-128.
Available from: DOI:10.1080/00986448608911401.

[17] SEDAHMED, G. H., M. A. KHATAB, F. M. MAHGOB and M. R. AL-AZZONY. SOLID-LIQUID MASS TRANSFER AT THE BASE OF A RECTANGULAR AGITATED VESSEL [online]. *Chemical Engineering Communications.* 2004, **191**(2), 168-181. Available from: DOI:10.1080/00986440390225242.

[18] KRESTA, Suzanne M., Deming MAO and Vesselina ROUSSINOVA. Batch blend time in square stirred tanks [online]. *Chemical Engineering Science.* 2006, **61**(9), 2823-2825. Available from: DOI:10.1016/j.ces.2005.10.069.

[19] GÓMEZ, C., C. P. J. BENNINGTON and F. TAGHIPOUR. Investigation of the Flow Field in a Rectangular Vessel Equipped With a Side-Entering Agitator [online]. *Journal of Fluids Engineering.* 2010, **132**(5). Available from: DOI:10.1115/1.4001575.

[20] CHTOUROU, W., M. AMMAR, Z. DRISS and M. S. ABID. CFD Prediction of the Turbulent Flow Generated in Stirred Square Tank by a Rushton Turbine [online]. *Energy and Power Engineering.* 2014, **06**(05), 95-110. Available from: DOI:10.4236/epe.2014.65010.

[21] SINGH, Buta, Zoltán SZAMOSI and Zoltán SIMÉNFALVI. State of the art on mixing in an anaerobic digester: A review [online]. *Renewable Energy.* 2019, **141**, 922-936. Available from: DOI:10.1016/j.renene.2019.04.072.

[22] AMEUR, Houari. Agitation of yield stress fluids in different vessel shapes [online]. *Engineering Science and Technology, an International Journal.* 2016, **19**(1), 189-196. Available from: DOI:10.1016/j.jestch.2015.06.007.

[23] AMMAR, M., Z. DRISS, W. CHTOUROU and M. S. ABID. Effect of the Tank Design on the Flow Pattern Generated with a Pitched Blade Turbine [online]. *International Journal of Mechanics and Applications.* 2012, **2**(1), 12-19. Available from: DOI:10.5923/j.mechanics.20120201.03.

[24] TACĂ, Constantin Dan and Mihaela PĂUNESCU. Suspension of solid particles in spherical stirred vessels [online]. *Chemical Engineering Science.* 2000, **55**(15), 2989-2993. Available from: DOI:10.1016/S0009-2509(99)00436-4.

[25] LEBRANCHU, Aline, Stéphane DELAUNAY, Philippe MARCHAL, Fabrice BLANCHARD, Stéphane PACAUD, Michel FICK and Eric OLMOS. Impact of shear stress and impeller design on the production of biogas in anaerobic digesters [online]. *Bioresource technology.* 2017, **245**(Pt A), 1139-1147. Available from: DOI:10.1016/j.biortech.2017.07.113.

[26] FOŘT, Ivan, Pavel SEICHTER, Luboš PEŠL, František RIEGER and Tomáš JIROUT. BLENDING CHARACTERISTICS OF HIGH-SPEED ROTARY IMPELLERS [online]. *Chemical and Process Engineering.* 2013, **34**(4), 427-434. Available from: DOI:10.2478/cpe-2013-0035.

[27] MEDEK, Jaroslav and Ivan FOŘT. Pumping effect of impellers with flat inclined blades [online]. *Collection of Czechoslovak Chemical Communications.* 1979, **44**(10), 3077-3089. Available from: DOI:10.1135/cccc19793077.

[28] FOSSETT, H. and L. E. PROSSER. The Application of Free Jets to the Mixing of Fluids in Bulk [online]. *Proceedings of the Institution of Mechanical Engineers.* 1949, **160**(1), 224-232. Available from: DOI:10.1243/PIME_PROC_1949_160_024_02.

[29] HARNBY, N., ed. *Mixing in the process industries.* 2nd ed., paperback ed. Oxford : Butterworth-Heinemann, 1997. 0 7506 3760 9.

[30] PATWARDHAN, Ashwin W. and Amit R. THATTE. Process Design Aspects of Jet Mixers [online]. *The Canadian Journal of Chemical Engineering.* 2004, **82**(1), 198-205. Available from: DOI:10.1002/cjce.5450820126.

[31] MARUYAMA, TOSHIRO, YUJI BAN and TOKURO MIZUSHINA. Jet mixing of fluids in tanks [online]. *JOURNAL OF CHEMICAL ENGINEERING OF JAPAN.* 1982, **15**(5), 342-348. Available from: DOI:10.1252/jcej.15.342.

[32] BUMRUNGTHAICHAICHAN, Eakarach. A review on numerical consideration for computational fluid dynamics modeling of jet mixing tanks [online]. *Korean Journal of Chemical Engineering.* 2016, **33**(11), 3050-3068. Available from: DOI:10.1007/s11814-016-0236-x.

[33] PERRY, Robert H., Don W. GREEN and James O. MALONEY, ed. *Perry's chemical engineers' handbook.* 7th ed. / prepared by a staff of specialists under the editorial direction of late editor, Robert H. Perry / editor, Don W. Green / associate editor, James O. Maloney. New York, London: McGraw-Hill, 1997. ISBN: 0-07-049841-5.

[34] VASSILATOS, George and H. L. TOOR. Second-order chemical reactions in a nonhomogeneous turbulent fluid [online]. *AIChE Journal.* 1965, **11**(4), 666-673. Available from: DOI:10.1002/aic.690110419.

[35] *NIST Chemical Kinetics Database* [cit. 24. May 2022]. Available from: https://kinetics.nist.gov/kinetics/Search.jsp.

[36] ZWIETERING, Th.N. Suspending of solid particles in liquid by agitators [online]. *Chemical Engineering Science.* 1958, **8**(3-4), 244-253. Available from: DOI:10.1016/0009-2509(58)85031-9.

[37] THE COMPRESSED AIR BLOG. *The Compressed Air Blog* [online]. 27. May 2022 [cit. 27. May 2022]. Available from: https://www.thecompressedairblog.com/the-real-value-of-compressed-air.

# List of figures



# List of tables